ANALYSIS OF THRUST DEVELOPMENT IN A PULSE DETONATON ENGINE

by

KISHORE NEKKANTI

Presented to the Faculty of the Graduate School of

The University of Texas at Arlington in Partial Fulfillment

of the Requirements

for the Degree of

MASTER OF SCIENCE IN AEROSPACE ENGENEERING

THE UNIVERSITY OF TEXAS AT ARLINGTON

May 2010

ACKNOWLEDGEMENTS

I would like to express my deep and sincere gratitude to my supervisor, Dr. Donald Wilson, whose encouragement, guidance and support from the initial to the final level enabled me to develop an understanding of the subject. I would like to thank Dr. Frank K. Lu for his guidance and support throughout this work. I would like to thank Dr. A. Haji Sheikh for serving on my committee and reviewing my thesis.

I owe my deepest gratitude to my colleagues, Eric Braun and Dr. Philip Panicker, for their advice and helpful discussions.

This thesis would not have been possible unless with the help of my friends Suneel Jinnala, Aditya, Harshan Ravi, Vamsi Vegunta and Siddarth Kashyap. I would like to thank all of these for their guidance in Matlab and Fluent.

I would like to show my gratitude to my friends Satya Bhanu, Raghu Ghandikota, Poornima Mynampati, Rajiv Kunisetty and Moyeen Shariff for their support and encouragement.

I am indebted to my father, mother and sister for their love and encouragement throughout my life.

April 15, 2010

ABSTRACT

ANALYSIS OF THRUST DEVELOPMENT

IN A PULSE DETONATON ENGINE

Kishore Nekkanti, M.S

The University of Texas at Arlington, 2010

Supervising Professor: Donald Wilson

Pulse detonation engines (PDE) employ detonation waves to compress and burn the fuel and oxidizer mixture which results in the release of high pressure and temperature. The objective of the present study is to analytically model the PDE cycle and to study the pressure, temperature, velocity and density distributions during the Taylor rarefaction wave, reflected rarefaction wave and the blow down process.

A two-dimensional supersonic nozzle is designed analytically by using the method of characteristics. The average values of nozzle thrust for one PDE cycle are calculated analytically using the impulse function and thrust coefficient. The variation of PDE thrust with the change in altitude is studied by designing the nozzle for two design points.

TABLE OF CONTENTS

LIST OF ILLUSTRATIONS

Figure Page

LIST OF TABLES

CHAPTER 1

INTRODUCTION

The invention of pulse jets in the late nineteenth century is credited to Martin Wiberg[1], a Swedish engineer. The first fully operational pulse jet was in fact built by a German engineer, Paul Schmidt[2], in 1930. The Germans were the first to develop pulse jet engines during World War II as they offered many advantages in terms of simplicity in design and low cost of manufacturing and production. The Germans developed a VTOL aircraft powered by the pulse jets towards the end of the World War II which never made into production line. They developed a cruise missile known as V-1 'Buzz Bomb' using the pulse jet engine technology which was used extensively during World War II. Small pulsejets engines can operate at up to 250 Hz. However, there are disadvantages of using pulse jet engines, namely loud noise, low fuel efficiency and heavy vibrations. Pulse jets are mainly of two types; mechanical valved pulse jets which use valves to control the filling of the fuel-air mixture and valveless pulsejets in which the filling of fuel and air is controlled aerodynamically by the pressure induced inside the combustion chamber. The limitations in the design of pulse jet engines have been greatly overcome by the invention of the pulse detonation engines (PDE).

A PDE can be operated at up to Mach 5; however higher Mach numbers can be theoretically achieved by employing unsteady detonation wave propagation in a supersonic flow. The major challenges in developing the PDE are to achieve detonations in a short distance and to reduce noise. The detonation can be achieved by using the deflagration to detonation transition (DDT) process. PDE employ detonation waves to compress and burn the fuel and oxidizer mixture which results in the release of high pressure, temperature and available power when compared to that of pulse jet engines. Since the detonation is supersonic, energy release

occurs at a fast rate. The thrust produced by the engine depends on various factors such as the number of detonation tubes, area of cross section of each tube, frequency of operation and exit velocity of the exhaust gases. The pulse detonation engines can be integrated in to rockets to achieve high performance, which at present uses the conventional deflagration process.

Between 1952 and 1956, Nicholls[3] et al. at the University of Michigan, Ann Arbor, used the idea of intermittent detonations and executed single-shot shock tube detonations and multi-cycle detonations using hydrogen/oxygen and acetylene/oxygen mixtures and concluded that the PDE can be a viable propulsion system. They also listed advantages such as simplicity in design, thrust availability from static condition through supersonic velocities, higher thrust levels and lower fuel consumption over pulsejets. L.J. Krzycki[4] conducted experiments on the design of a PDE using propane-air mixture operating at 60 Hz. The results of the study were published in a paper in June 1962, and Krzycki concluded that the reason for low operating frequencies and low thrust production was due to the filling times. In 1986, Helman[5] et al. published a paper which explained the basic operational concepts and advantages of PDE. They designed the PDE in such a way that the detonation wave propagates into the combustor and then reflects back. They predicted that PDE could be widely used for space and atmospheric vehicles by 2000. In the 1990s, Bussing[6] performed experimental studies of single and multi combustor PDE using different fuels such as ethylene and hydrogen. Current research on PDEs is conducted using CFD. On January 31st, 2008, the first PDE-powered flight took off at the Mohave Desert Air and Space Port in California[7].

1.1 Thermodynamic Cycles

1.1.1 *Brayton Cycle*

The Brayton cycle was proposed by George Brayton around 1870[8]. This cycle assumes constant pressure combustion (deflagration burning) and is the basis for all gas turbine engines. The T-s diagram of Brayton cycle is shown in Fig 1.1. In the Brayton cycle, first the free stream air that enters through the inlet is compressed isentropically from state (1-3). The compressed

air then enters the combustion chamber where the temperature is increased by an assumed constant pressure heat addition (combustion) from state 3 to 4. Then the gas from the combustion chamber is expanded isentropically in the turbine from state 4 to 5. The exhaust from the turbine is further expanded isentropically in a nozzle to ambient conditions from state 5 to 6. The efficiency of the Brayton cycle is given by[9]

$$\eta_{th} = 1-(T_o/T_3)$$

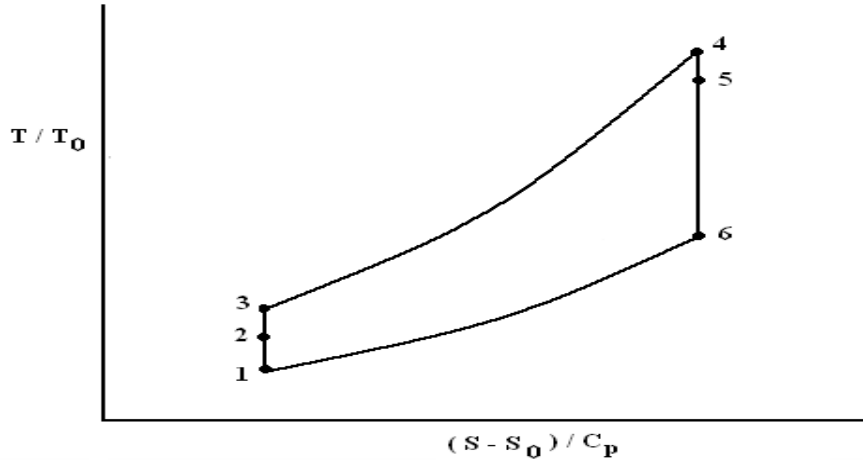

Fig 1.1 T – s diagram of Brayton cycle[9]

1.1.2 *Humphrey cycle*

The Humphrey cycle is identical to the Brayton cycle except that the constant pressure heat addition process is replaced by a constant volume heat addition process. The thermal efficiency of the Humphrey cycle is less than that of the PDE cycle. The thermal efficiency is given by[9].

$$\eta_{th} = 1 - (1/\hat{q})\left[(1+\gamma\hat{q}/\varphi)^{1/\gamma} - 1\right] \quad (1)$$

where $\hat{q} = f^*h_{PR} / C_pT_o$ (1a)

$$\varphi = T_3/T_o$$

(1b)

1.1.3 *PDE Cycle*

The PDE cycle is identical to the Brayton cycle except for the combustion process. The ZND model for the PDE is shown[9] from point 3 to 4 in Fig 1.2. In this process, the detonation wave is comprised of a shock wave which moves at the Chapman-Jouguet detonation velocity and increases the temperature and pressure (generally referred to as the von Neumann spike). Immediately following the shock wave, there exist regions where chemical reactions occur. This region is thicker than that of a shock wave. The shock wave heats up the reactants to such a high temperature that they react among themselves resulting in detonation. Since the thickness of the shock wave is very small, we assume limited reactions to occur within the shock wave region. Thus, the profiles of pressure, temperature and density parameters are flat in the region behind the shock front. This region is termed as the induction zone. After this zone, the reaction rate increases resulting in the properties of gas reaching an equilibrium state (at the end of reaction). This zone is termed as the reaction zone. The Taylor rarefaction wave, which follows the termination of the CJ region, is produced between the end of the reaction zone and boundary wall of the chamber. The amount of heat addition and the initial conditions determine the properties of shock wave from point 3-3a. The local Mach number at point 4 is determined by the Chapman-Jouguet condition. The detonation mixture is then expanded isentropically via a reflected expansion wave from the open end of the tube. The efficiency of the PDE cycle is given by[9]

$$\eta_{th} = 1 - \left[\frac{1}{{M_{CJ}}^2} \left(\frac{1 + \gamma {M_{CJ}}^2}{\gamma + 1} \right)^{\frac{(\gamma+1)}{\gamma}} - 1 \right] \Big/ \hat{q}$$

(2)

where $\hat{q}$ = f*h_{PR} / $C_p T_o$

(2a)

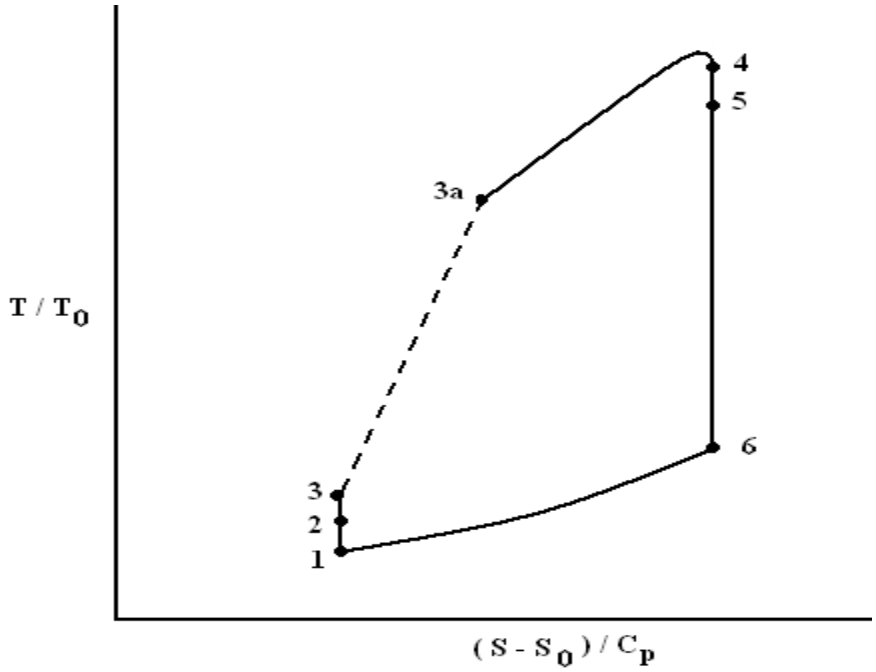

Fig 1.2 T-s diagram of PDE cycle[9]

The three ideal cycles are compared with respect to their T-s cycle diagram and thermal efficiency in the following figures. Note that a common compression from state 1 to 3 is assumed for all three cycles.

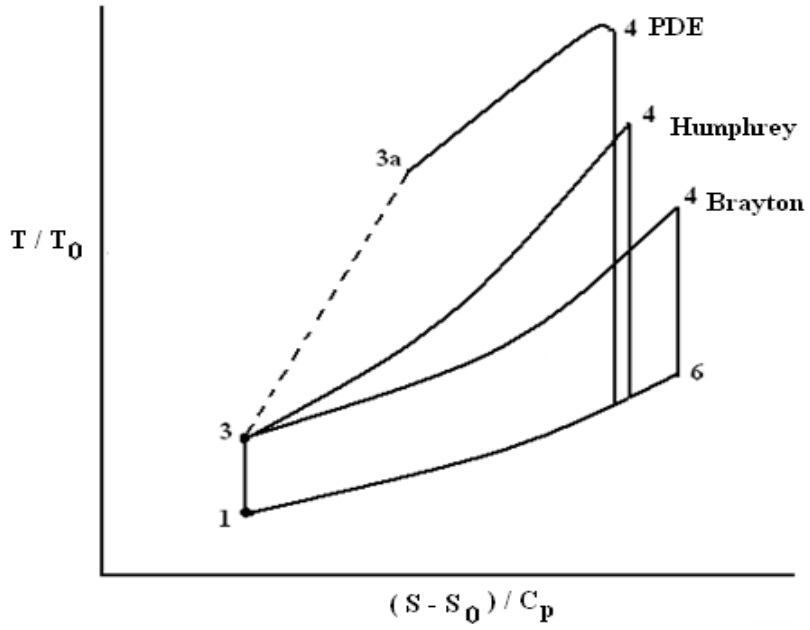

Fig 1.3 T-S diagrams of Brayton, Humphrey and PDE cycles[9]

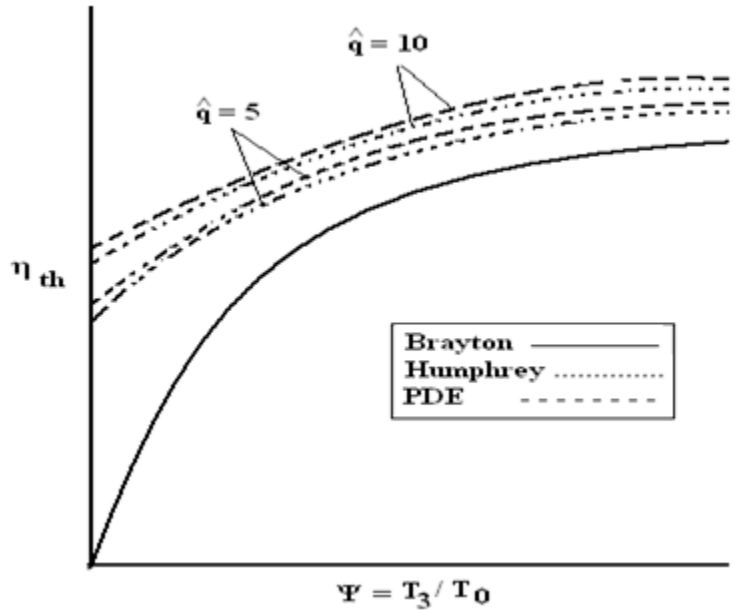

Fig 1.4 Thermal efficiency of, Brayton Humphrey and PDE cycles[9]

From the above graphs we can conclude that the Ideal PDE cycle has a thermal efficiency advantage over the Brayton and Humphrey cycles. The thermodynamic cycle

efficiency of the PDE cycle is in the range of 0.4 to 0.8, which is higher than that of Brayton cycle[9].

1.2 Detonation Theory

1.2.1 *Deflagration*

Deflagration is basically a combustion wave moving with subsonic speed. The deflagration waves propagate at a speed on the order of 1-100m/s. The fires we see in our daily life is usually deflagration. It is easier to control deflagration waves than detonation waves.

1.2.2 *Detonation*

Detonation is basically a combustion wave moving at supersonic speed. The detonation wave consists of a shock wave which is very thin on the order of a few mean free paths of the gas molecules. Due to this fact, much of the reactions occur behind the shock wave region. The detonation wave propagate through the medium at a supersonic speed of about 2000 m/s. Detonation waves are generally modeled by the Chapman-Jouguet theory and the ZND theories. The main differences between the detonation and deflagration are listed in the Table 1.1 below.

Table 1.1 Differences between detonation and deflagration[10]

	Detonation	Deflagration
M_1	>1	<1
M_2	≤ 1	<1
$\frac{V_2}{V_1}$	<1	>1
$\frac{P_2}{P_1}$	>1	<1
$\frac{\rho_2}{\rho_1}$	>1	<1
$\frac{T_2}{T_1}$	>1	<1

1.2.3 *Chapman- Jouguet Theory*

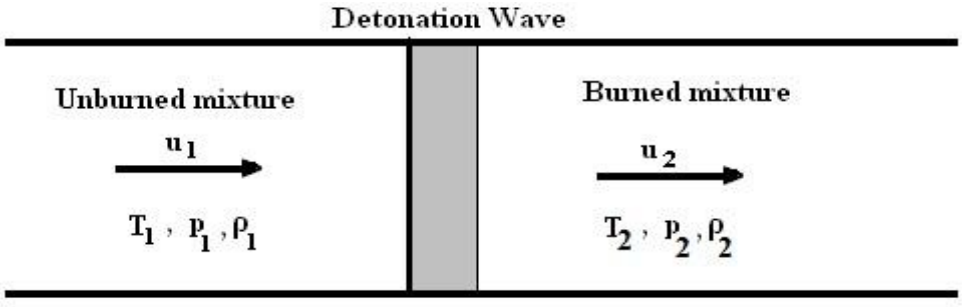

Fig 1.5 Schematic of stationary one-dimensional combustion wave[11]

By assuming steady one-dimensional flow in the detonation wave reference frame, and applying the continuity, momentum and energy equations to the control volume enclosing the detonation wave, we can obtain the following relations between the unburned and burned states[11].

$$\rho_1 u_1 = \rho_2 u_2 = \dot{m} \tag{3}$$

$$p_1 + \rho_1 {u_1}^2 = p_2 + \rho_2 {u_2}^2 \tag{4}$$

$$h_1 + \frac{1}{2}{u_1}^2 = h_2 + \frac{1}{2}{u_2}^2 \tag{5}$$

By combining the above obtained equations we obtain the Rankine-Hugoniot relation[11].

$$p_2 - p_1 = \rho_1 {u_1}^2 - \rho_2 {u_2}^2 = \frac{(\rho_1 u_1)^2}{\rho_1} - \frac{(\rho_2 u_2)^2}{\rho_2} = \left(\frac{1}{\rho_1} - \frac{1}{\rho_2}\right)\dot{m}^2 \tag{6}$$

The Rayleigh line is a straight line obtained by connecting points corresponding to the initial and final states on a graph of pressure versus specific volume for a substance subjected to a shock wave and its relation is[11].

$$\rho_1{}^2 u_1{}^2 = \frac{p_2 - p_1}{1/\rho_1 - 1/\rho_2} = \dot{m}^2 \tag{7}$$

$$\frac{\gamma}{\gamma - 1}\left(\frac{p_2}{\rho_2} - \frac{p_1}{\rho_1}\right) - \frac{1}{2}(p_2 - p_1)\left(\frac{1}{\rho_1} + \frac{1}{\rho_2}\right) = q \tag{8}$$

$$h_2 - h_1 = \frac{1}{2}(p_2 - p_1)\left(\frac{1}{\rho_1} + \frac{1}{\rho_2}\right) \tag{9}$$

The study of deflagration and detonation waves can be understood by using the Hugoniot curve.

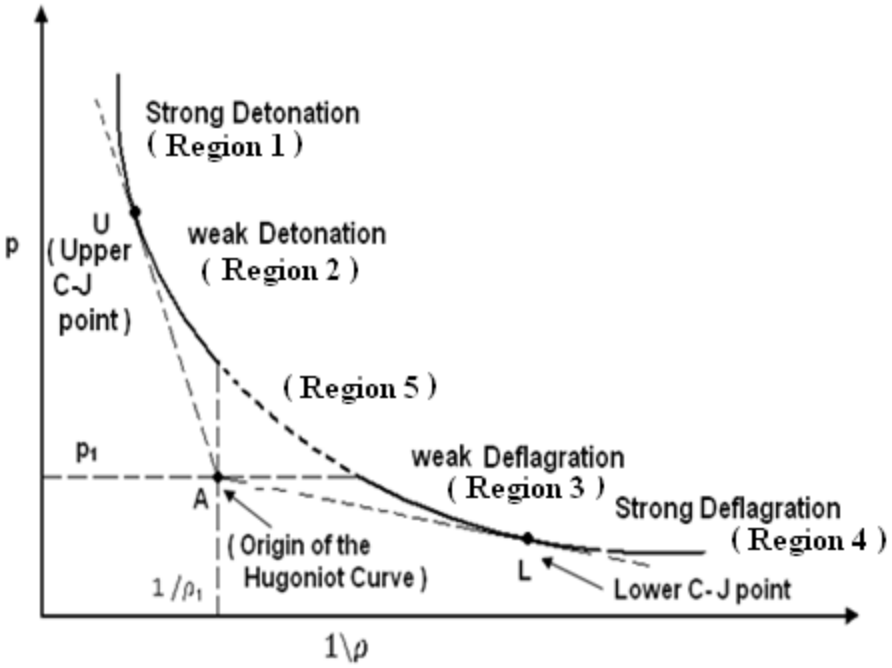

Fig 1.6 Hugoniot curve[11]

The different regions in the Hugoniot curve are constructed using the Rayleigh lines drawn as a tangent line from point A to the Hugoniot curve with the tangency points U and L

which are called the Chapman-Jouguet points and also a vertical and horizontal line from point A which divides the Hugoniot curve in to 5 regions[11].

Region 1 is considered to be the strong detonation region where the pressure of the burned gases is greater than the C-J detonation wave pressure. When the gas passes through a strong detonation wave, the velocity of the gas decreases significantly from supersonic to subsonic speed, while the density and pressure of the gases increases.

Region 2 is considered to be the weak-detonation region where the pressure of the burned gas is smaller than the C-J detonation wave pressure. When the gases pass through the weak detonation wave, the velocity of the gas decreases, but it is still supersonic.

Region 3 is considered to be the weak deflagration region. When the gas passes through this region; the velocity increases from a subsonic velocity to a higher subsonic velocity, while the pressure in the burned gas zone is less than that of unburned gas zone.

Region 4 is a strong deflagration region. When the burned gases pass through the strong deflagration region the velocity of burned gases is increased from subsonic to a higher subsonic speed.

Region 5 is the region wherein the value of the velocity is obtained to be imaginary, derived from the Rayleigh expression. Therefore it is impossible to physically realize this region.

1.2.4 *ZND Theory*

The Zel'dovich-von Neumann-Doring (ZND) theory is an extension of the classical Chapman-Jouguet theory. This theory assumes the flow to be one-dimensional in nature and steady in relation to the detonation front. The detonation wave comprises of a thin shock wave which moves at the detonation velocity, followed by a thicker region in which chemical reactions occur. It is also assumed that the thickness of the shock wave is usually in the order of a few mean free paths of the gas molecules, resulting in limited chemical reactions in the shock wave region. Fig 1.7 depicts the variation in the physical properties within the ZND detonation wave. In the region behind the shock front the profiles of temperature, density and pressure exhibit a

relatively flat nature. This region is termed the induction zone. After the induction zone, the chemical reaction rates increase greatly and the thermodynamic properties ultimately approach the equilibrium C-J state, in a region termed as the reaction zone. As the products expand, the temperature rises from the von Neumann state to the Chapman-Jouguet state and the pressure decreases in the reaction zone. Further, a rarefaction, known as the Taylor rarefaction wave, is produced between the end of the reaction zone and boundary wall of the chamber[11].

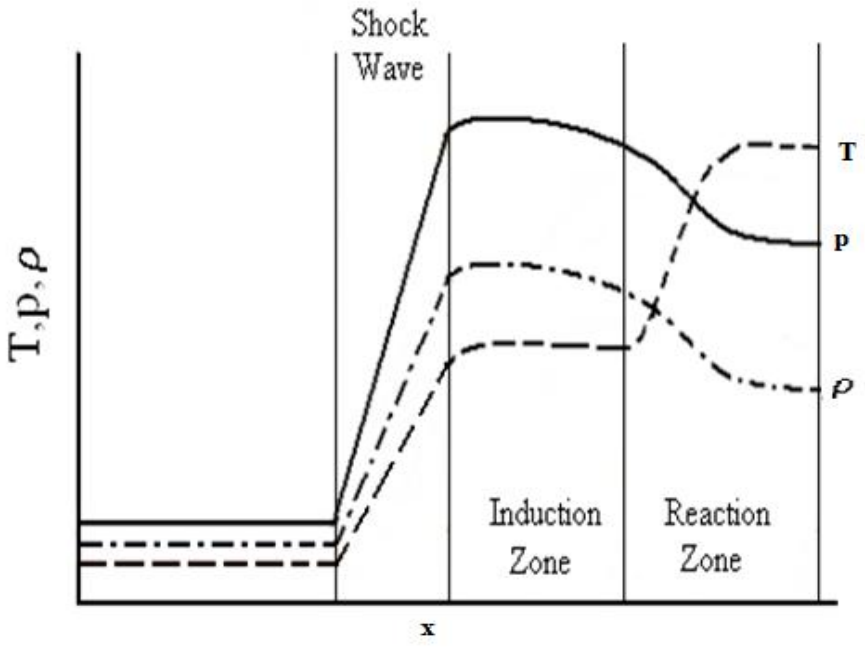

Fig 1.7 Schematic of variation of physical properties through a ZND detonation wave[11]

CHAPTER 2

ANALYTICAL MODEL OF PDE

A pulse detonation engine is basically designed as a long cylindrical tube which is closed at one end and open at the other end. The PDE is provided with inlets for injecting fuel and oxidizer. The initial detonation wave is produced via the DDT process. The operation of the PDE can be understood by the Fig 2.1 given below which will be described later.

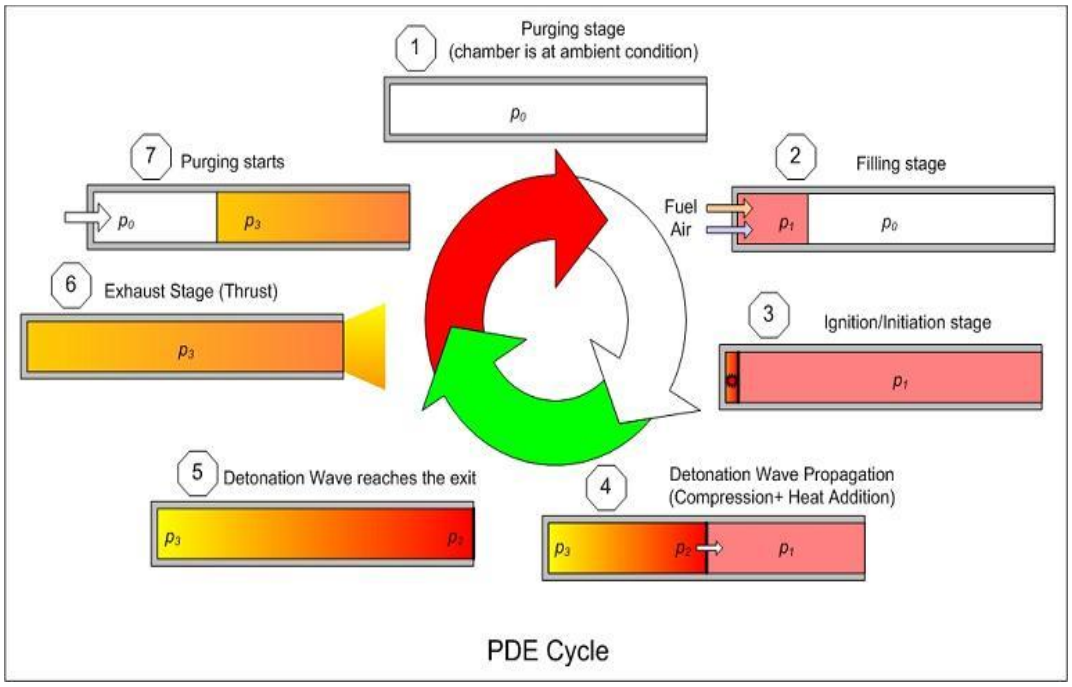

Fig 2.1 Schematic of PDE cycle process[12]

In the following sections, the model developed by Endo and Fujawara[13, 14] is described.

2.1 Filling process

The filling process involves filling up the PDE tube with the fuel-air mixture at a certain required velocity: see stage 2 of cycle in Fig 2.1. The time required for this process to occur should be minimized as even a small delay can ultimately decrease the cycle-averaged thrust and efficiency. The CJ detonation wave is ignited at the closed end, i.e. x=0 at time t=0, and immediately starts propagating towards the open end. The filling time can be computed using the following expression

$$t_{fill} = \frac{length\ of\ the\ tube}{filling\ velocity} = \frac{L}{v_{fill}} \tag{10}$$

The fuel-oxidizer mixture is pumped into the detonation tube with a velocity termed as filling velocity v_{fill}. If the flow velocity is higher, the filling time would be reduced which ultimately reduces the cycle time.

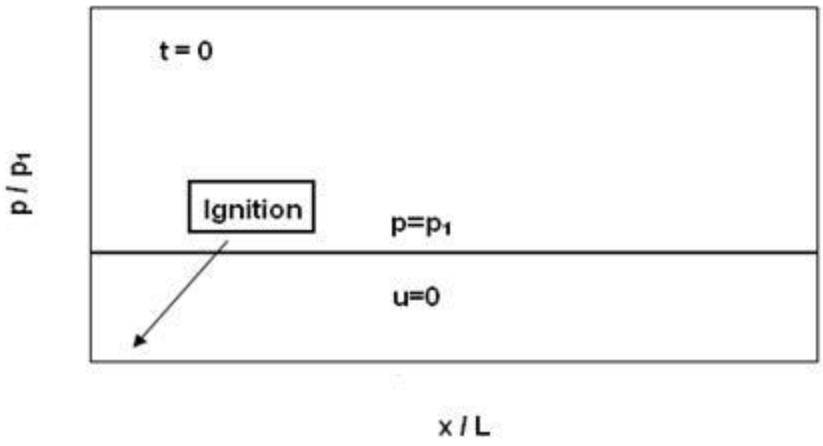

Fig 2.2 Pressure and velocity distribution at t = 0[13]

2.2 CJ Detonation Wave

This is the process that occurs immediately after the filling process. When the fuel and oxidizer mixture ignites, the detonation wave is produced which propagates towards the open end of the tube from the location x = 0.When the detonation wave propagates towards the open end from the closed end, it also induces the gas downstream of the detonation wave to flow towards the open end. This behavior results since the detonation wave possesses the properties of a compression wave. The CJ surface of the detonation wave is located at the position x_2 which is given by[13]

$$x_2=D_{CJ}t \tag{11}$$

The properties of the CJ surface of detonation wave are given by[13]

$$\rho_2 = 2\left(\frac{\gamma_2 + 1}{2\,\gamma_2}\right)\rho_1 \tag{12}$$

$$p_2 = \gamma_1 M_{CJ}^2 p_1/(\gamma_2 + 1) \tag{13}$$

$$u_2 = a_2/\gamma_2 = D_{CJ}/(\gamma_2 + 1) \tag{14}$$

The detonation wave consists of a shock wave that moves with the velocity of detonation wave. The peak pressure behind the shock wave is called von Neumann spike. The properties of the von Neumann spike are given by[13]

$$\rho_N = \frac{\gamma_1+1}{\gamma_1-1}\rho_1 \tag{15}$$

$$P_N = \frac{2\gamma_1}{\gamma_1 + 1} M^2{}_{CJ} P_1 \tag{16}$$

The detonation wave propagates from the open end to the closed end with a velocity referred to as the CJ detonation velocity. The time required for the detonation wave to travel can be computed using the expression given by[13]

$$\frac{t_1}{2} = \frac{length\ of\ the\ tube}{CJ\ wave\ velocity} = \frac{L}{D_{cj}} \tag{17}$$

2.3 Taylor rarefaction wave

As the detonation wave moves towards the open end, the gas flow between the C-J detonation wave and the closed end is decelerated to zero velocity to satisfy the solid wall boundary condition at the closed end of the tube. This ultimately results in generation of a rarefaction wave which follows the detonation wave[13] which is shown in Fig 2.3.

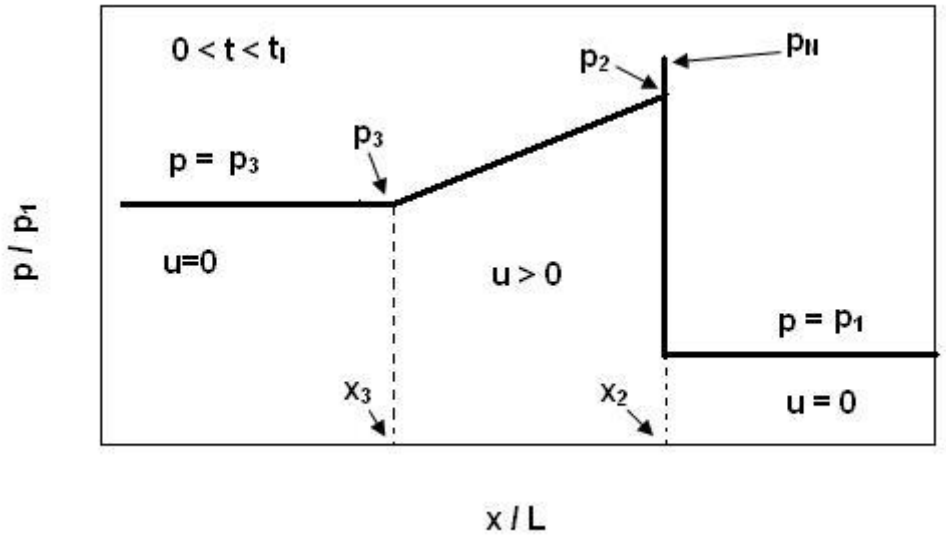

Fig 2.3 Pressure distribution at 0< t< t_1[13]

The properties at the front boundary of the rarefaction wave are identical to the properties of CJ surface of the detonation wave. The time taken by the trailing edge of the rarefaction wave to reach the end of the detonation tube is given by[13]

$$t_1 = \frac{length\ of\ the\ tube}{\left(\frac{Detonation\ velocity}{2}\right)} = \frac{L}{\left(\frac{D_{cj}}{2}\right)}$$

(18)

The rear boundary of rarefaction wave is located at the position x = x_3. The location of x_3 is given by the expression[13]

$$X_3 = D_{CJ}\frac{t}{2}$$

(19)

The properties of the rear boundary of rarefaction wave are given by the following expressions[13]

$$a_3 = \frac{D_{CJ}}{2}$$

(20)

$$\rho_3 = 2\left(\frac{\gamma_2 + 1}{2\gamma_2}\right)^{\frac{\gamma_2+1}{\gamma_2-1}}\rho_1$$

(21)

$$p_3 = \frac{\left(\frac{\gamma_2 + 1}{2\gamma_2}\right)^{\frac{\gamma_2+1}{\gamma_2-1}}}{2}\frac{\gamma_1}{\gamma_2}{M_{CJ}}^2 p_1$$

(22)

$$U_3 = 0$$

(23)

The distribution of the gas dynamic properties within the Taylor rarefaction wave are given by the following relations[13]

$$\rho = \left(\frac{1}{\gamma_2} + \frac{\gamma_2 - 1}{\gamma_2}\frac{x}{x_2}\right)^{\frac{2}{\gamma_2-1}}\rho_2$$

(24)

$$p = \left(\frac{1}{\gamma_2} + \frac{\gamma_2 - 1}{\gamma_2}\frac{x}{x_2}\right)^{\frac{2\gamma_2}{\gamma_2 - 1}} \rho_2$$

(25)

$$u = u_2 - \frac{2}{\gamma_2 + 1}\frac{x_2 - x}{t} = -a + \frac{x}{t}\left(\leq \frac{1}{\gamma_2}a\right)$$

(26)

$$a = a_2 - \frac{\gamma_2 - 1}{\gamma_2 + 1}\frac{x_2 - x}{t}$$

(27)

2.4 Reflected rarefaction wave

At time t = t_1 the Taylor rarefaction wave reaches the open end and the burned gases will occupy the entire tube. The pressure distribution in the tube at time t = t_1 is shown in Fig 2.4.

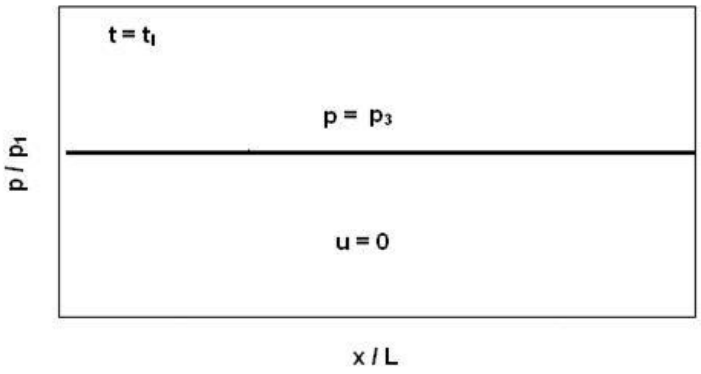

Fig 2.4 Pressure distribution at time t=t_1[13]

When the rarefaction wave exits the tube a reflected rarefaction wave propagates back into the tube from the open end and moves towards closed end within the time $t_1 < t < t_2$. The time t_2 is given by[13]

$$t_2 = \frac{4L}{D_{CJ}}$$

(28)

The properties of gas inside the reflected rarefaction wave are given by following expressions[13]

$$\rho = \left(1 + \frac{\gamma_2 - 1}{D_{CJ}} \frac{L - x}{t - t_I}\right)^{\frac{2}{\gamma_2 - 1}} \rho_{ex} \tag{29}$$

$$p = \left(1 + \frac{\gamma_2 - 1}{D_{CJ}} \frac{L - x}{t - t_I}\right)^{\frac{2\gamma_2}{\gamma_2 - 1}} p_{ex} \tag{30}$$

$$u = u_{ex} - \frac{2}{\gamma_2 + 1} \frac{L - x}{t - t_I} = a - \frac{L - x}{t - t_I} (\leq a) \tag{31}$$

$$a = a_{ex} + \frac{\gamma_2 - 1}{\gamma_2 + 1} \frac{L - x}{t - t_I} \tag{32}$$

where

$$\rho_{ex} = \frac{\gamma_2 + 1}{\gamma_2^{\frac{\gamma_2 + 1}{\gamma_2 - 1}}} \rho_1 \tag{32a}$$

$$p_{ex} = \frac{\gamma_1}{\gamma_2^{\frac{2\gamma_2}{\gamma_2 - 1}} (\gamma_2 + 1)} M_{CJ}{}^2 p_1 \tag{32b}$$

$$u_{ex} = a_{ex} = \frac{1}{\gamma_2 + 1} D_{CJ} \tag{32c}$$

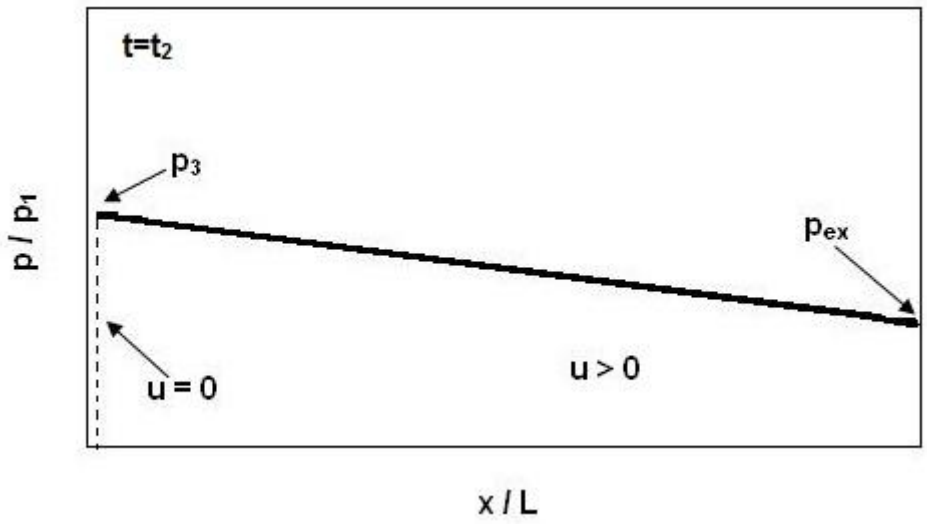

Fig 2.5 Pressure distribution at time t = t_2[13]

2.5 Exhaust process

This process exhausts the burned gas from the open end of the tube. Endo and Fujiwara[13], assumed the pressure decreases linearly with time, until it reached ambient conditions. In a subsequent paper[14], the pressure at the closed end is assumed to decay exponentially as the front boundary of reflected rarefaction wave reaches the closed end which is shown in Fig 2.6. The exhaust phase ends when the thrust density decays to pressure p_1.

When the reflected rarefaction wave reaches the closed end of the tube the velocity at the closed end is u = 0. At this case using the continuity equation and differentiating Euler's equation by x we obtain the following equations[14]

$$\frac{dP_w}{dt} = -\gamma_2 \left(\frac{\partial u}{\partial x}\Big|_{x=0}\right) P_w \tag{33}$$

and

$$\left(\frac{\partial u}{\partial x}\Big|_{x=0}\right)^2 = -\frac{1}{\rho_3} \left(\frac{\partial^2 P}{\partial x^2}\Big|_{x=0}\right) \left(\frac{P_3}{P_w}\right)^{1/\gamma_2} \tag{34}$$

Using the approximation

$$\left.\frac{\partial^2 P}{\partial x^2}\right|_{x=0} = -\lambda^2 \frac{P_w}{L^2} \tag{35}$$

where

$$\lambda = \frac{2^{k_{III}} \sqrt{\gamma_2}}{(\gamma_2+1)^{k_{III}} - 2^{k_{III}}} \tag{35a}$$

We obtain the following equation

$$\frac{dP_w}{dt} = -\lambda\, \gamma_2 \frac{P_3{}^{1/(2\gamma_2)}}{L\sqrt{\rho_3}} P_w{}^{k_{II}+1} \tag{36}$$

When $t = t_2$, $P_w = P_3$. Then the relation for P_w is given by[14]

$$P_w = P_3 \left[\frac{\frac{1}{\gamma}\frac{4\sqrt{\gamma_2}}{\gamma_2-1} t_{CJ}}{\left(t - t_{plateau}\right) + \frac{1}{\gamma}\frac{4\sqrt{\gamma_2}}{\gamma_2-1} t_{CJ}} \right]^{1/k_{II}} \tag{37}$$

The flow field parameters of the reflected rarefaction wave just before the arrival of the front boundary at the closed end are given by[14]

$$\int_0^L \rho\, dx = \rho_3 \left[1 - \left(\frac{2}{\gamma_2+1}\right)^{k_{III}}\right] L \tag{38}$$

$$(\rho u)|_{x=L} = \frac{2^{2/(\gamma_2-1)}}{(\gamma_2+1)^{k_{III}}} \rho_3 D_{CJ} \tag{39}$$

Using these parameters we obtain the following equation[14]

$$\left(\frac{dP_w}{dt}\right)\Big|_{t=t_2} = -\frac{2^{2/\gamma_2-1}}{(\gamma_2+1)^{k_{III}}-2^{k_m}}\frac{\gamma_2 P_3}{t_{CJ}} \tag{40}$$

The thrust density P_w is given by[14]

$$P_w = \begin{cases} p_3 & (0 \le t \le t_{II}) \\ p_3\left[\dfrac{k_{IV}t_{CJ}}{(t-t_{II})+k_{IV}t_{CJ}}\right]^{\frac{2\gamma_2}{\gamma_2-1}} & (t_{II} \le t \le t_{Exhaust}) \end{cases} \tag{41}$$

Where

$$k_{IV} = \left(\frac{2\left[\left(\gamma_2\frac{\gamma_2+1}{2\gamma_2}\right)^{\frac{\gamma_2+1}{\gamma_2-1}}-1\right]}{\gamma_2\frac{\gamma_2-1}{2\gamma_2}}\right) \tag{42}$$

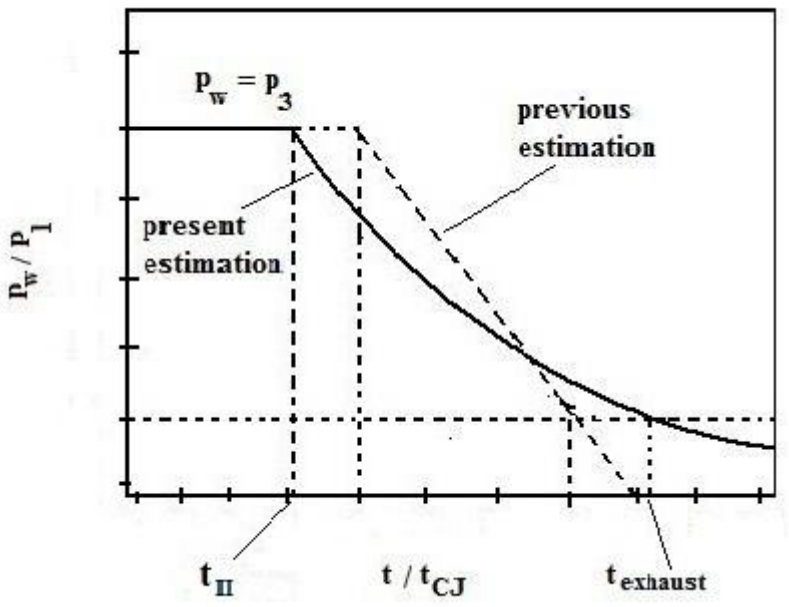

Fig 2.6 Pressure on the thrust wall as a function of time[14]

2.6 Purging process

The purging process involves pumping of air in to the detonation tube at high velocities which purges residual combustion products from the tube so that a fresh fuel/oxidizer mixture can be injected into the tube by the time $t=t_{cyc}$. If the length of the tube is L and the purge velocity V_{purge}, the time taken for the process to complete is given by the following expression

$$t_{purge} = L / V_{purge}$$

With higher purge velocities, lower purge times and faster cycle times can be accomplished. The impulse density per one cycle is given by[14]

$$I_{cyc} = \int_0^{t_{exhaust}} p_w \, dx = K_{II} p_3 t_{CJ} \tag{43}$$

where

$$K_{II} = 2\left(\frac{\gamma_2+1}{2\gamma_2}\right)^{\frac{\gamma_2+1}{\gamma_2-1}/2} + \frac{(k_{IV})}{\frac{\gamma_2+1}{\gamma_2-1}}\left[1 - \left(\frac{K_I - 2\left(\frac{\gamma_2+1}{2\gamma_2}\right)^{\frac{\gamma_2+1}{\gamma_2-1}/2}}{\frac{2\left[\left(\gamma_2\frac{\gamma_2+1}{2\gamma_2}\right)^{\frac{\gamma_2+1}{\gamma_2-1}}-1\right]}{\gamma_2\frac{\gamma_2-1}{2\gamma_2}}} + 1\right)^{\frac{\gamma_2+1}{\gamma_2-1}}\right] \tag{43a}$$

and $k_{IV} = \left(\frac{2\left[\left(\gamma_2\frac{\gamma_2+1}{2\gamma_2}\right)^{\frac{\gamma_2+1}{\gamma_2-1}}-1\right]}{\gamma_2\frac{\gamma_2-1}{2\gamma_2}}\right)$ (43b)

$$K_I = \frac{2\left[\left(\gamma_2\frac{\gamma_2+1}{2\gamma_2}\right)^{\frac{\gamma_2+1}{\gamma_2-1}}-1\right]}{\gamma_2\frac{\gamma_2-1}{2\gamma_2}}\left[\left(\frac{1}{2}\frac{\gamma_1}{\gamma_2}\right)^{\frac{\gamma_2-1}{2\gamma_2}}\frac{\gamma_2+1}{2\gamma_2}^{\frac{\gamma_2+1}{2\gamma_2}} M_{CJ}{}^{2\frac{\gamma_2-1}{2\gamma_2}} - 1\right] + 2\left(\frac{\gamma_2+1}{2\gamma_2}\right)^{\frac{\gamma_2+1}{\gamma_2-1}/2} \tag{43c}$$

The specific- Impulse I_{sp} is given by[14]

$$I_{sp} = \frac{I_{cyc}}{\emptyset \rho_1 L g} \tag{44}$$

where ∅ = equivalence ratio

CHAPTER 3

ANALYTICAL ANALYSIS OF PDE

The analytical analysis of the PDE has been studied based on the analytical model given by Takuma Endo and Toshi Fujiwara[13] in Chapter 2. A spreadsheet is prepared in order to analyze the PDE performance.

3.1 Initial Conditions

The governing initial free stream conditions are selected in accordance with the desired fuel and oxidizer mixture. Table 3.1 gives the different initial condition parameters chosen in the design of PDE. The fuel and oxidizer selected for the analysis are H_2 and O_2.

Table 3.1 Initial conditions chosen for PDE analysis

Initial conditions			
Pressure	P1	atm	1.0
Temperature	T1	K	300.000
Fuel			H2
Oxidizer			O2
Equivalence ratio	ϕ		1.000
Enthalpy	h1	kJ/kg	4.470
Molecular weight	MW1	kJ/(kg.mol.K)	12.010
Specific heat ratio	gamma1		1.401
Speed of sound	a1	m/s	539.500
Density	ρ1	kg/m^3	0.488
Gas constant	R1	J/(kg.K)	692.308
g		m/s^2	9.800

3.2 CJ conditions

CEA is a program which calculates the concentration of chemical equilibrium products (chosen from any set of reactants) and determines the thermodynamic and transport properties of the mixture. The CEA program is used instead of the Takuma Endo and Toshi Fujiwara[13] relations to calculate the Chapman-Jouguet detonation parameters. The Cj conditions obtained from CEA code are show in the Table 3.2.

Table 3.2 CJ conditions from NASA CEA code

CJ conditions (from NASA CEA code)			
Detonation Mach number	M(CJ)		5.256
Detonation wave speed	D(CJ)=D2	m/sec	2835.700
Pressure	P(CJ)=P2	atm	18.904
Temperature	T(CJ)=T2	K	3675.810
Density	rhoCJ)=Rho2	kg/m^3	0.897
Enthalpy(CEA)	h-cj (h2)	J/kg	2835.400
Molecular weight	MW2	kJ/(kg.mol.K)	14.500
Specific heat	Cp2	kJ/(Kg.K)	16.250
Specific heat ratio	gamma2		1.129
Sonic velocity	a(CJ)=a2	m/sec	1542.500
Velocity, u2	u(CJ')=u2	m/s	1366.495
Gas constant	R2	J/(kg.K)	573.400

3.3 Von Neumann spike

The point at which the Rayleigh line intersects with the Hugoniot of the unreacted explosive is termed as the Von Neumann spike. The important parameters such as pressure, temperature, density ratios are calculated at this point which are shown in the Table 3.3.

Table 3.3 Von Neumann spike conditions

Von Neumann Spike (from CEA/NS Calculations)			
Pressure Ratio	p2/p1		32.764
Temperature ratio	T2/T1		5.882
Density ratio	ρ_{2/ρ_1}		5.570
Pressure	P(VN)	atm	32.764
Temperature	T(VN)	K	1764.600
Density	rho(VN)	kg/m^3	2.717
Mach number*	M(VN)		0.411
rho(VN)			
Gas constant, R_2	R_2	J/(kg.K)	692.335
Speed of sound, a_2	a_2	m/s	1308.466
Velocity, u_2*	u_2	m/s	538.172
density-NS	rho_2	kg/m^3	2.717

* - with respect to moving shock reference frame

3.4 End wall conditions

The properties of the gas at the rear boundary of the rarefaction wave are calculated and are shown in the Table 3.4 which characterizes the gas in the region $o<x<x_L$.

Table 3.4 End wall conditions

End Wall (station 3) conditions			
Wave Speed	D3	m/s	1417.850
Pressure	P3	atm	6.495
Density	ρ_3	kg/m^3	0.370
Temperature	T3	K	3105.932
Time when Detonation exit the open end	t 1	sec	0.000705
Time for Rerefraction wave from open to closed end	t 2	sec	0.001411

3.5 Detonation Taylor rarefaction wave

The state of flow inside the rarefaction wave is determined as shown in the Table (3.5). Also, the velocity, pressure, temperature and density distributions are shown within the time $0<t<t_1$.

$\frac{t_1}{2}$= time when detonation wave is at exit of tube

t_1 = time when Taylor rarefaction wave exits tube.

Table 3.5 Properties of Taylor rarefaction wave

Detonation/ Taylor Rarefraction Wave (0<t<t1)												
Distance	x	m	0.0	0.1	0.2	0.3	0.4	0.5	0.6	0.7	0.8	0.9	1.0
Pressure	P	atm	6.495	6.495	6.495	6.495	6.495	6.495	8.336	10.266	12.613	15.460	18.904
Pressure	p	Pa	658130.769	658130.769	658130.769	658130.769	658130.769	658130.769	844609.944	1040229.729	1278025.931	1566433.915	1915447.800
Density	ρ	kg/m^3	0.360	0.360	0.360	0.360	0.360	0.360	0.434	0.522	0.627	0.750	0.897
Temperature	t1	K	3186.152	3186.152	3186.152	3186.152	3186.152	3186.152	3392.319	3473.921	3556.493	3640.035	3724.547
Detonation Tube Length	L	m	1.000										
time t1		ms	0.705										
Time, t		ms	0.000	0.071	0.141	0.212	0.282	0.353	0.423	0.494	0.564	0.635	0.705
1-x		m	1.000	0.900	0.800	0.700	0.600	0.500	0.400	0.300	0.200	0.100	0.000
Local Velocity	u	m/s	0.000	0.000	0.000	0.000	0.000	0.000	478.452	795.610	1033.479	1218.488	1366.495
	X/X2		0.000	0.100	0.200	0.300	0.400	0.500	0.600	0.700	0.800	0.900	1.000
CJ Wave Location	X2 = D2*t	m	0.000	0.200	0.400	0.600	0.800	1.000	1.200	1.400	1.600	1.800	2.000
Trailing wave Location	X3 = X2/2	m	0.000	0.100	0.200	0.300	0.400	0.500	0.600	0.700	0.800	0.900	1.000
Velocity Distribution (t=t1/2)		m/s	0.000	0.000	0.000	0.000	0.000	0.000	478.452	795.610	1033.479	1218.488	1366.495
Velocity Distribution (t=t1)			0.000	0.000	0.000	0.000	0.000	0.000	0.000	0.000	0.000	0.000	0.000
Acoustic Speed Distribution (t=t1/2)		m/s	1417.850	1417.850	1417.850	1417.850	1417.850	1417.850	1485.310	1505.735	1521.054	1532.968	1542.500
Acoustic Speed Distribution (t=t1)			1417.850	1417.850	1417.850	1417.850	1417.850	1417.850	1417.850	1417.850	1417.850	1417.850	1417.850
Density Distribution (t=t1/2)		kg/m^3	0.370	0.370	0.370	0.370	0.370	0.370	0.434	0.522	0.627	0.750	0.897
Density Distribution (t=t1)			0.370	0.370	0.370	0.370	0.370	0.370	0.370	0.370	0.370	0.370	0.370
Pressure Distribution (t=t1/2)		atm	6.495	6.495	6.495	6.495	6.495	6.495	8.336	10.266	12.613	15.460	18.904
Pressure Distribution (t=t1)			6.495	6.495	6.495	6.495	6.495	6.495	6.495	6.495	6.495	6.495	6.495
Temperature Distribution (t=t1/2)		k	3186.152	3186.152	3186.152	3186.152	3186.152	3186.152	3392.319	3473.921	3556.493	3640.035	3724.547
Temperature Distribution (t=t1)			3186.152	3186.152	3186.152	3186.152	3186.152	3186.152	3186.152	3186.152	3186.152	3186.152	3186.152

The variation of pressure with respect to length of the PDE tube for the time $t = \frac{t_1}{2}$ is shown in the Fig 3.1.

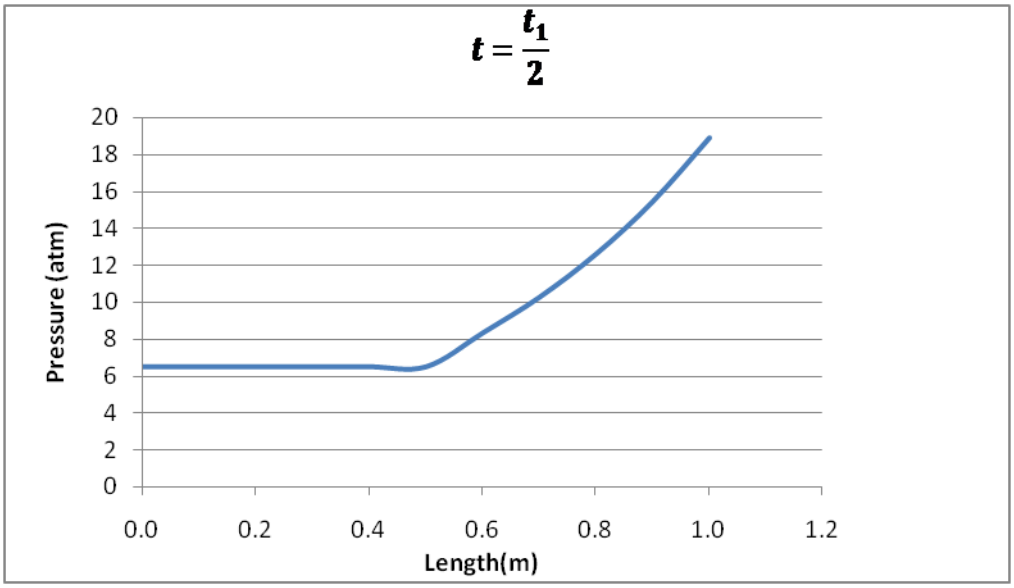

Fig 3.1 Variation in pressure at $t = \frac{t_1}{2}$ as detonation wave exits tube

The variation of pressure with respect to length of the PDE tube for the time $t = t_1$ is shown in the Fig 3.2.

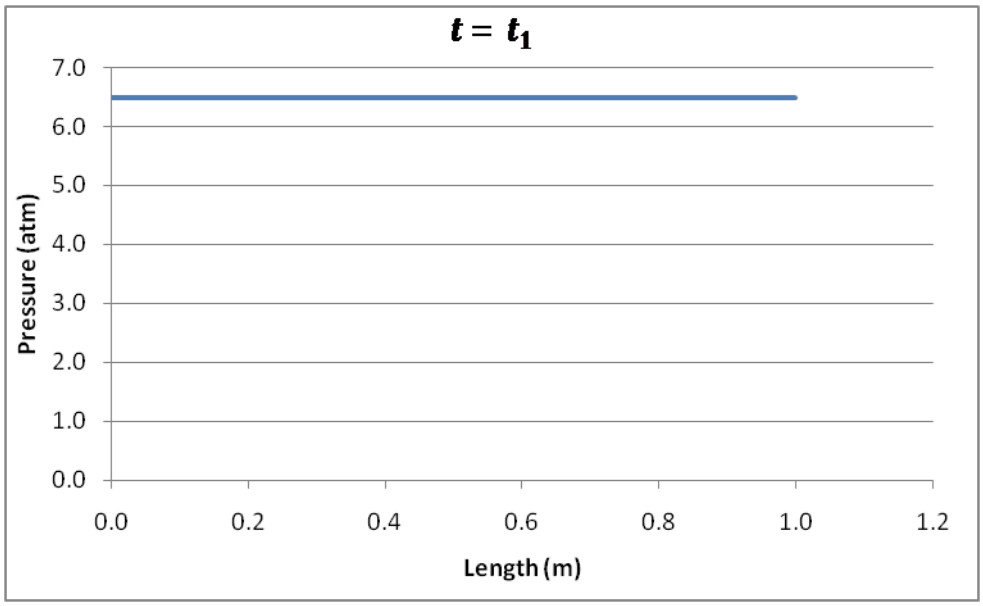

Fig 3.2 Variation in pressure at $t = t_1$ as Taylor rarefaction wave exits tube

The variation of density with respect to length of the PDE tube for the time $t = \frac{t_1}{2}$ is shown in Fig 3.3.

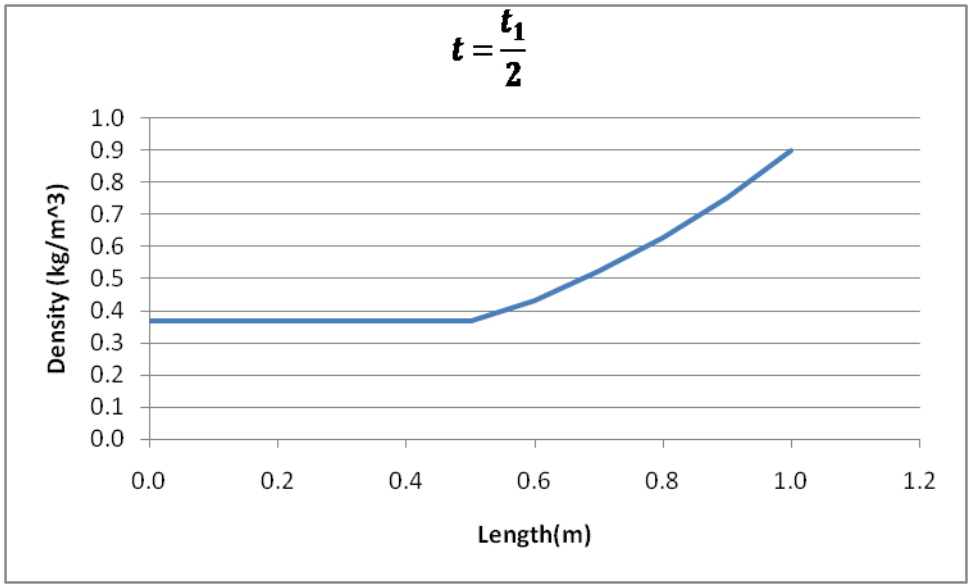

Fig 3.3 Variation in density at $t = \frac{t_1}{2}$ as detonation wave exits tube

The variation of density with respect to length of the PDE tube for the time $t = t_1$ is shown in Fig 3.4.

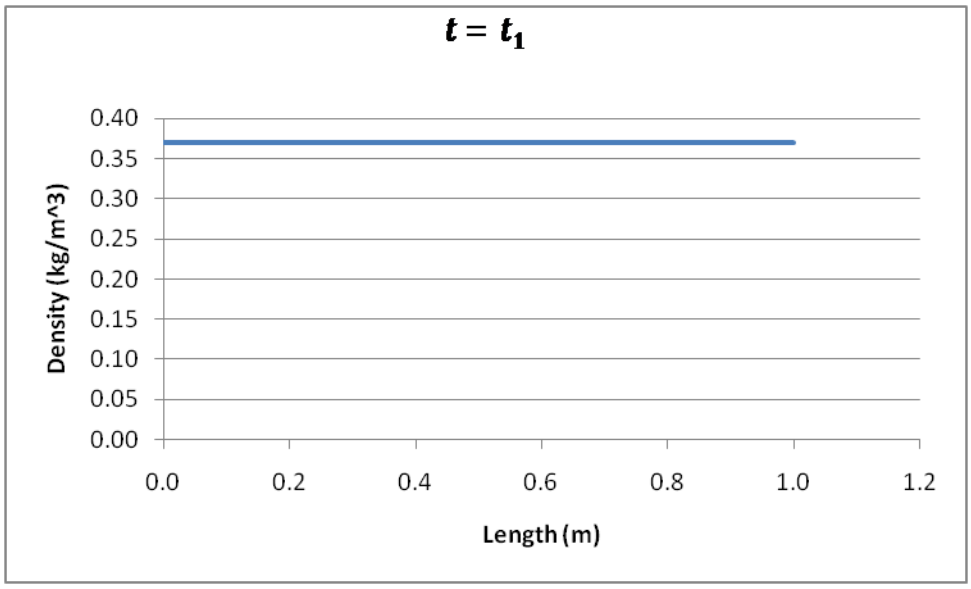

Fig 3.4 Variation in density at $t = t_1$ as Taylor rarefaction wave exits tube

The variation of temperature with respect to length of the PDE tube for the time $t = \frac{t_1}{2}$ is shown in Fig 3.5.

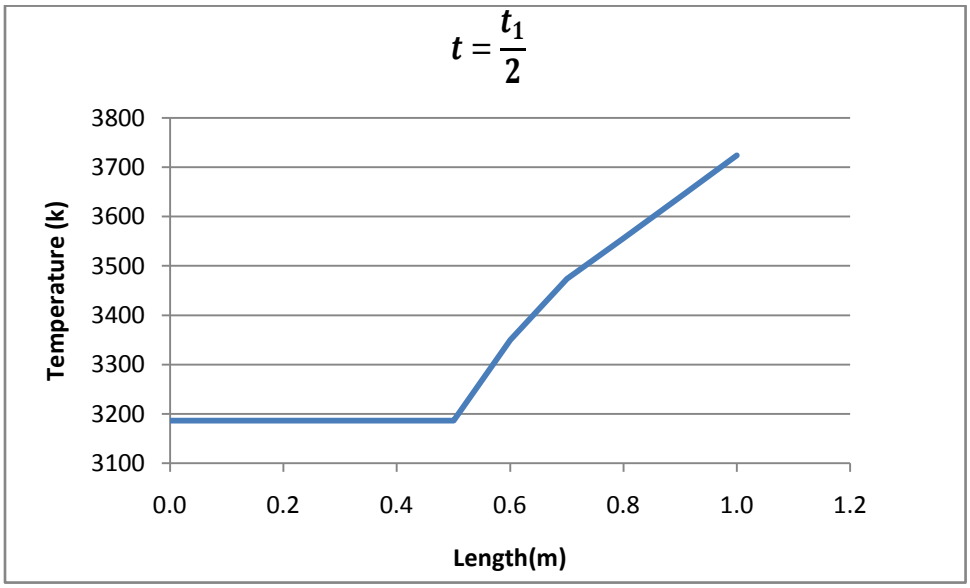

Fig 3.5 Variation in temperature at $t = \frac{t_1}{2}$ as detonation wave exits tube

The variation of Temperature with respect to length of the PDE tube for the time $t = t_1$ is shown in Fig 3.6.

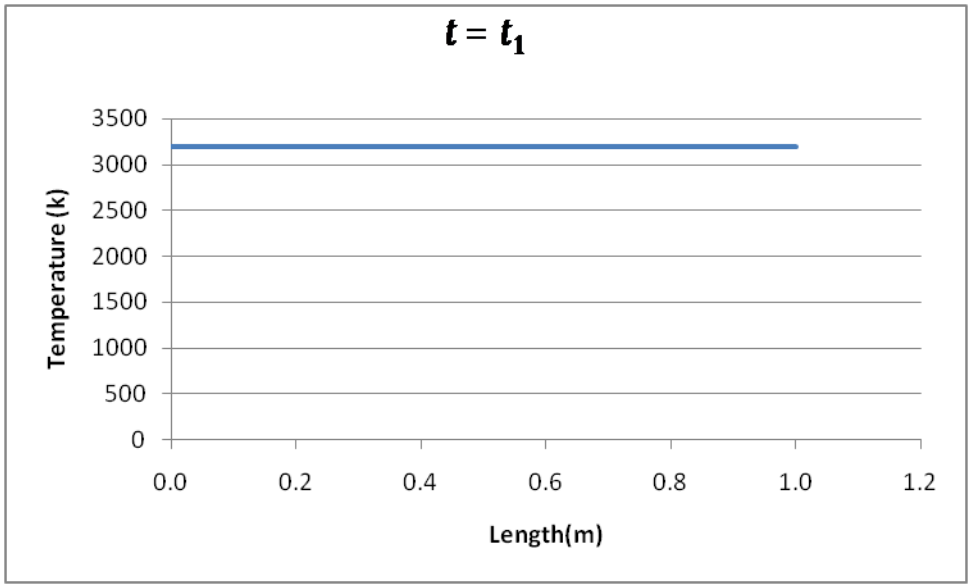

Fig 3.6 Variation in temperature at $t = t_1$ as Taylor rarefaction wave exits tube

3.6 Exhaust gas

A reflected rarefaction wave propagates from the open end to the closed end causing the burned gas to exhaust through the open end. The properties of the front boundary of the reflected rarefaction wave as calculated by the Takuma Endo and Toshi Fujiwara[13] model are summarized in Table 3.6 below.

Table 3.6 Exhaust gas conditions

Exhaust Gas (Station 3 Conditions)			
Pressure	Pex	atm	2.204
Density	ρ ex	kg/m^3	0.142
Velocity	Uex	m/s	1332.065
velocity of sound	a ex	m/s	1332.065

3.7 Reflected rarefaction wave

The distribution of the gas dynamic properties within the reflected rarefaction wave is determined in this section. The parameters such as pressure, temperature, density distributions are calculated as shown in Table 3.7.

Table 3.7 Properties of reflected rarefaction wave

Reflected Rarefraction wave t1< t<t2												
Time	t	S	0.000705	0.000775	0.000845	0.00092	0.00099	0.00106	0.00113	0.00120	0.00127	0.00134	0.00141
Distance	x	m	0.0	0.1	0.2	0.3	0.4	0.5	0.6	0.7	0.8	0.9	1.0
Length	L	m	1.000										
	L-x	m	1.0	0.9	0.8	0.7	0.6	0.5	0.4	0.3	0.2	0.1	0.0
Pressure	p	atm	6.495	6.495	6.495	6.495	6.495	6.495	4.570	3.518	2.884	2.467	2.175
Density	ρ	kg/m^3	0.360	0.360	0.360	0.360	0.360	0.372	0.271	0.215	0.180	0.157	0.140
Velocity	u	m/s	0.000	0.000	0.000	0.000	0.000	0.000	437.307	756.863	996.531	1182.939	1332.065
Speed of sound	a	m/s	1245.631	1245.631	1245.631	1245.631	1245.631	1245.631	1274.443	1295.022	1310.457	1322.461	1332.065
Temperature	T	K	3186.152	3186.152	3186.152	3186.152	3186.152	3083.950	2983.772	2896.055	2831.126	2781.135	2741.462
Velocity Distribution (t=(t2-t1)/2)		m/s	0.000	0.000	0.000	0.000	0.000	0.000	437.307	756.863	996.531	1182.939	1332.065
Velocity Distribution (t=t2-t1)			0.000	133.207	266.413	399.620	532.826	666.033	799.239	932.446	1065.652	1198.859	1332.065
Acoustic Speed Distribution (t=(t2-t1)/2)		m/s	1245.631	1245.631	1245.631	1245.631	1245.631	1245.631	1274.443	1295.022	1310.457	1322.461	1332.065
Acoustic Speed Distribution (t=t2)			1417.850	1409.272	1400.693	1392.115	1383.536	1374.958	1366.379	1357.801	1349.222	1340.644	1332.065
Density Distribution (t=(t2-t1)/2)		kg/m^3	0.377	0.377	0.377	0.377	0.377	0.372	0.271	0.215	0.180	0.157	0.140
Density Distribution (t=t2)			0.370	0.336	0.306	0.278	0.253	0.229	0.208	0.189	0.171	0.155	0.140
Pressure Distribution (t=(t2-t1)/2)		atm	6.495	6.495	6.495	6.495	6.495	6.495	4.570	3.518	2.884	2.467	2.175
Pressure Distribution (t=t2-t1)			6.495	5.840	5.247	4.711	4.228	3.791	3.397	3.042	2.722	2.434	2.175
Temperature Distribution (t=(t2-t1)/2)		k	3186.152	3186.152	3186.152	3186.152	3186.152	3083.950	2983.772	2896.055	2831.126	2781.135	2741.462
Temperature Distribution (t=t2)			3105.932	3068.462	3031.219	2994.204	2957.415	2920.855	2884.521	2848.416	2812.537	2776.886	2741.462

The variation of pressure with respect to length of the PDE tube at $t = t_1 + \frac{t_2 - t_1}{2}$ is shown in Fig 3.7.

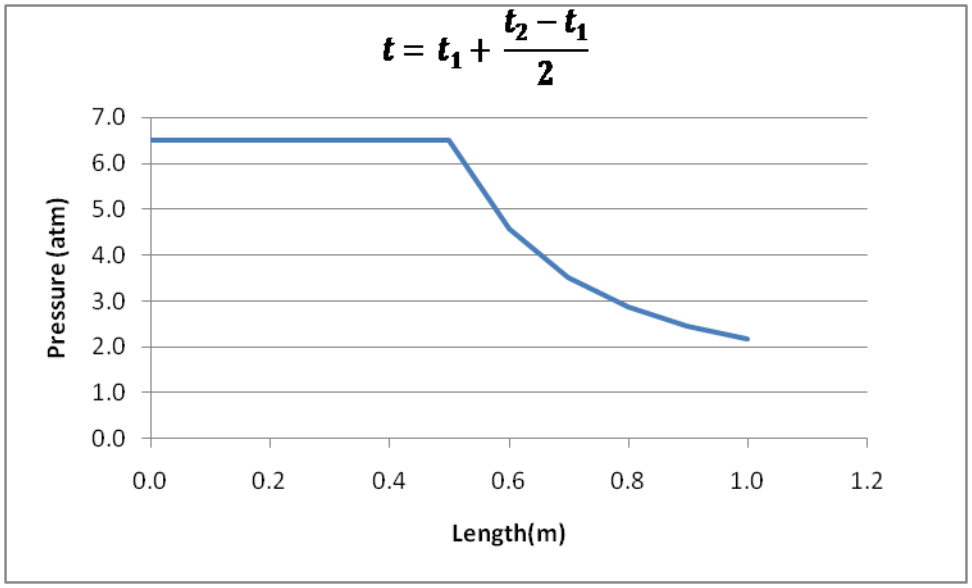

Fig 3.7 Variation in pressure at $t = t_1 + \frac{t_2 - t_1}{2}$ during reflected rarefaction wave

The variation of pressure with respect to length of the PDE tube at $t = t_2 - t_1$ is shown in Fig 3.8.

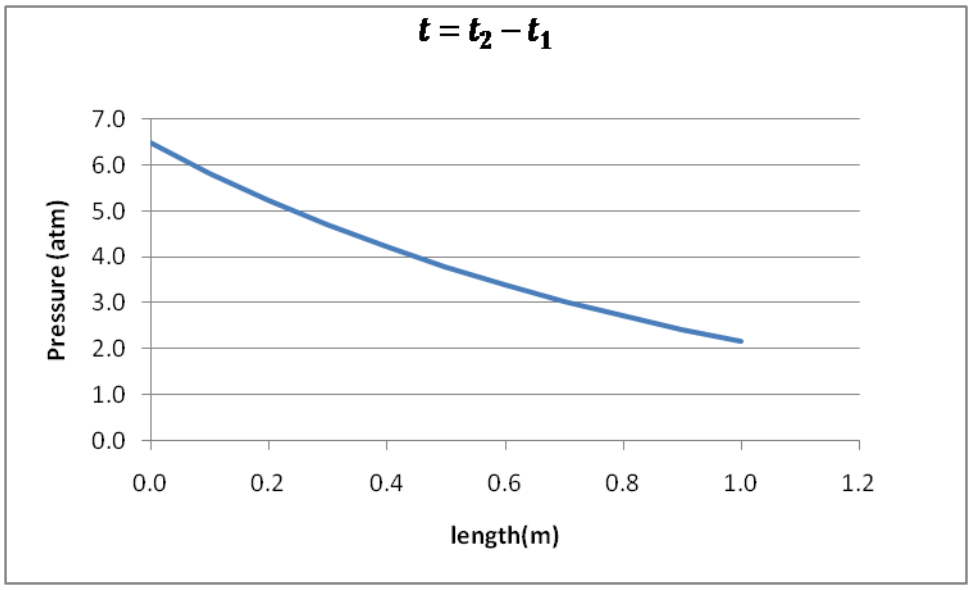

Fig 3.8 Variation in pressure at $t = t_2 - t_1$ during reflected rarefaction wave

The variation of density with respect to length of the PDE tube at $t = t_1 + \frac{t_2 - t_1}{2}$ is shown in Fig 3.9.

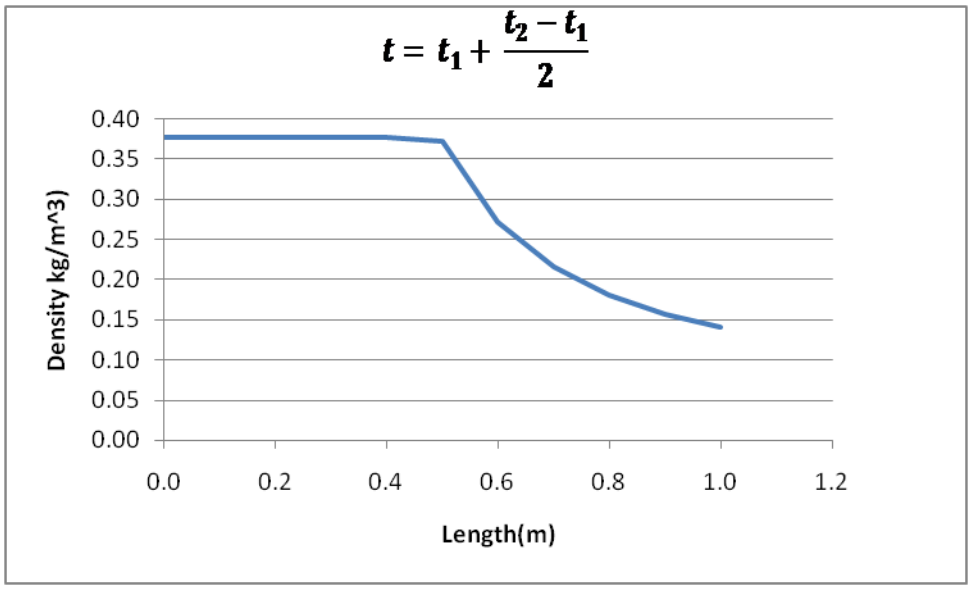

Fig 3.9 Variation in density at $t = t_1 + \frac{t_2 - t_1}{2}$ during reflected rarefaction wave

The variation of density with respect to length of the PDE tube at $t = t_2 - t_1$ is shown in Fig 3.10.

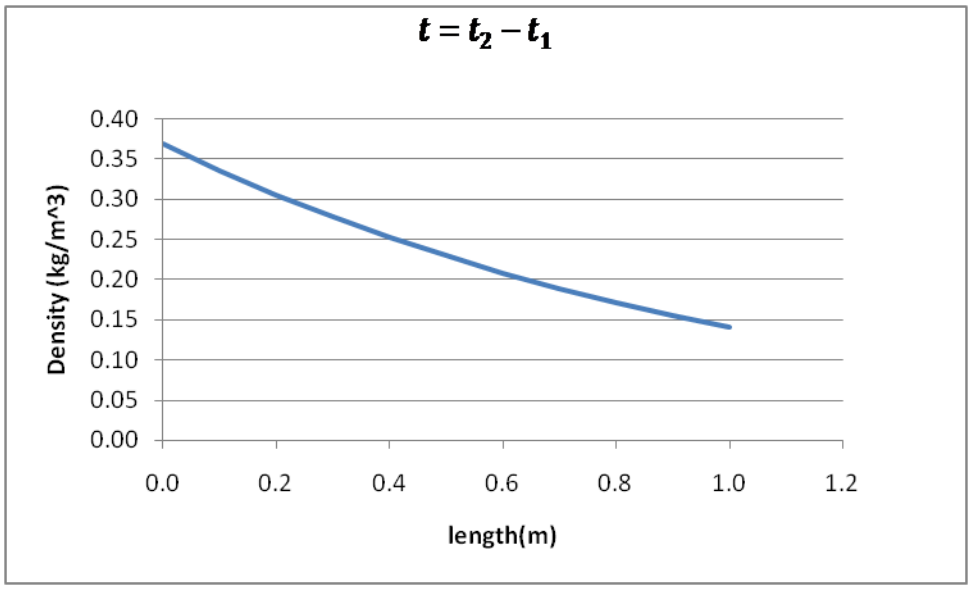

Fig 3.10 Variation in density at $t = t_2 - t_1$ during reflected rarefaction wave

The variation of temperature with respect to length of the PDE tube at $t = t_1 + \frac{t_2 - t_1}{2}$ is shown in Fig 3.11.

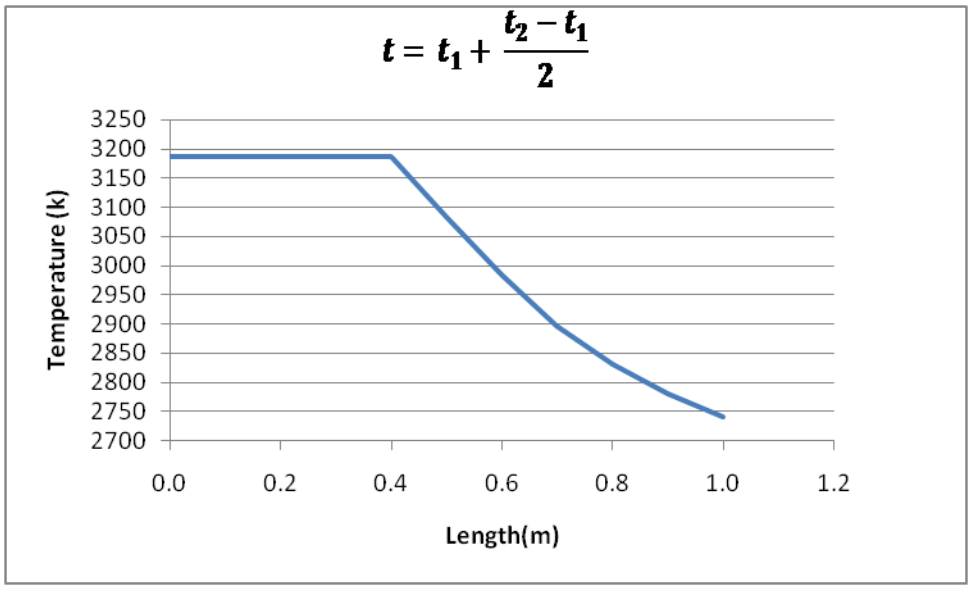

Fig 3.11 Variation in temperature at $t = t_1 + \frac{t_2 - t_1}{2}$ during reflected rarefaction wave

The variation of temperature with respect to length of the PDE tube at $t = t_2 - t_1$ is shown in Fig 3.12.

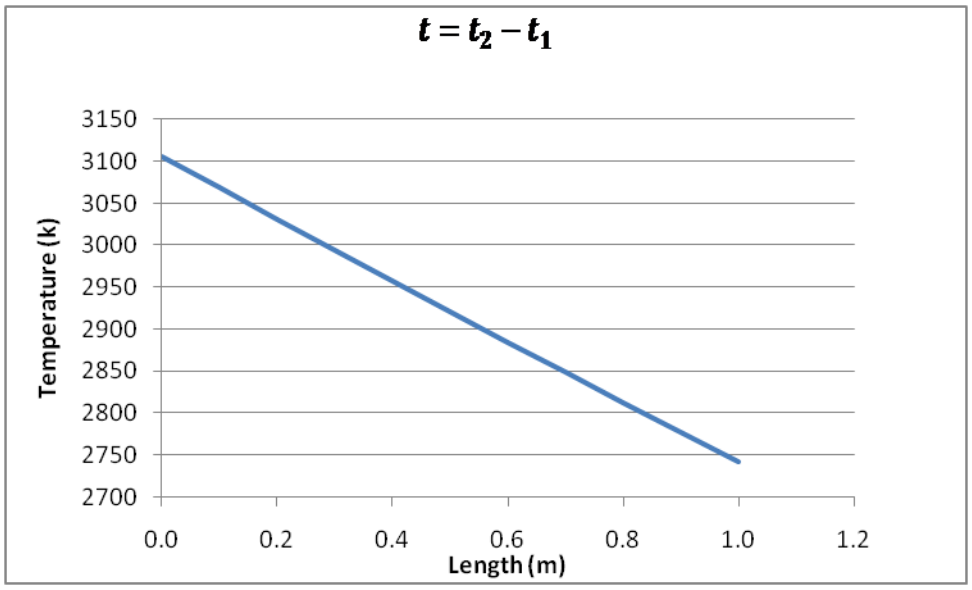

Fig 3.12 Variation in temperature at $t = t_2 - t_1$ during reflected rarefaction wave

3.8 Blow down process

The pressure at the closed end decays after the arrival of the front boundary of the rarefaction wave at the closed end. Table 3.8 shows results of the blow down process.

Table 3.8 Properties of Blow down process

BlowDown Process												
T plateau		s	0.002									
T exhaust		s	0.006									
0 ≤ t ≤ t plateau			0.000	0.0002	0.0004	0.0005	0.0007	0.0009	0.0011	0.0013	0.0014	0.0016	0.0020
Pressure	p	atm	6.495	6.495	6.495	6.495	6.495	6.495	6.495	6.495	6.495	6.495	6.495
t 2≤t ≤ t exhaust													
time			0.002	0.00261	0.00297	0.00333	0.00369	0.00405	0.00441	0.00477	0.00513	0.00549	0.006
Pressure	p	atm	6.495	5.382	4.480	3.745	3.144	2.650	2.242	1.904	1.623	1.387	1.190

The variation of pressure with respect to time during the blow down process is shown in Fig 3.13.

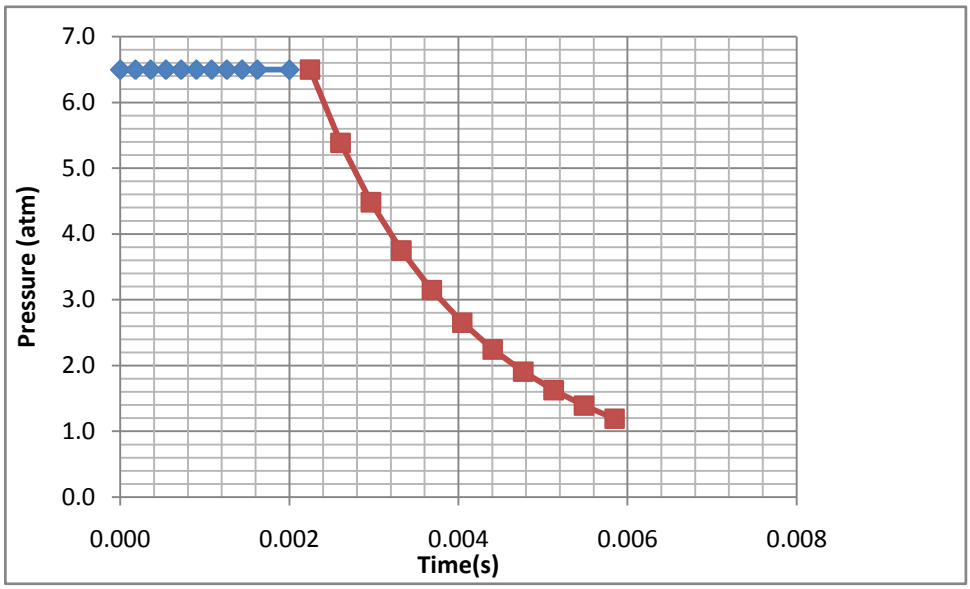

Fig 3.13 Variation in pressure during blow down process

CHAPTER 4

NOZZLE DESIGN

4.1 Theory of method of characteristics

The method of characteristics is often used to design two-dimensional exhaust nozzles. A characteristic curve is defined as the path of propagation of physical disturbances. These physical disturbances are propagated along Mach lines. In a supersonic flow, these Mach lines are called the characteristic lines[15].

The slope of the characteristic lines for 2-D steady, planar flow is given by[15]

$$\left(\frac{dy}{dx}\right)_{char} = \frac{-uv/a^2 \pm \sqrt{\mathrm{M}^2 - 1}}{[1 - (u^2/a^2)]} \tag{45}$$

By observing the value of M in the above equation the flow properties can be determined. For M>1, two real characteristics pass through each point in the flow field. For M=1, one real characteristic passes through each point in the flow field and for M<1, the characteristics are imaginary[15]. Since the characteristics are imaginary for subsonic steady flow, the method of characteristics technique is employed only for supersonic steady flows[15].

Consider the streamline geometry, as shown in the Fig 4.1, for a steady, two-dimensional supersonic flow.

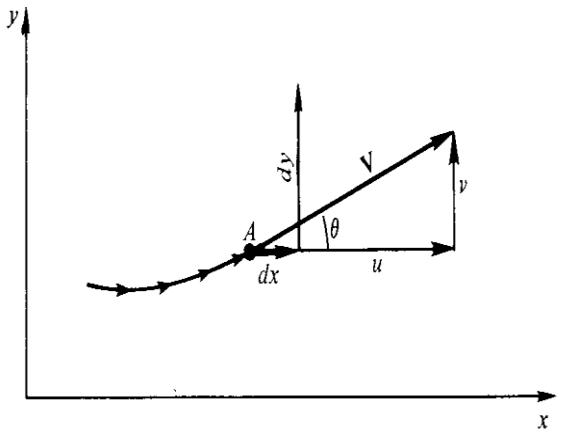

Fig 4.1 Streamline geometry[15]

Real characteristic lines are obtained from $\left(\frac{dy}{dx}\right)_{char}$. Examining these lines for the supersonic flow, the slope of the characteristic line is given by[15]

$$\frac{dy}{dx} = \tan\theta \pm \quad (46)$$

The above equation is represented graphically as shown in Fig 4.2. At each point along the streamline, which makes an angle θ with respect to x-axis as shown in Fig 4.2, two characteristics; one at an angle μ above the streamline and one at an angle μ below the streamline, passing through A. These lines are also called Mach lines. The characteristic given by angle θ+μ is called the C+ characteristic while the characteristic given by angle θ-μ is called the C- characteristic[15].

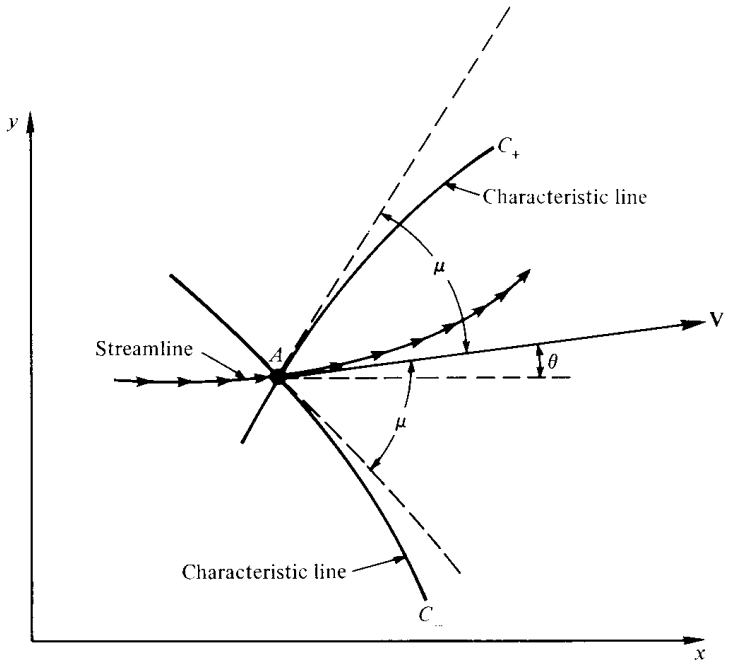

Fig 4.2 Schematic of left and right running characteristics[15]

The compatibility equations are the equations which govern the variation of the flow properties along the characteristic line. The compatibility equations are given by[15]

$$d\theta = -\sqrt{M^2 - 1}\frac{dV}{V} \quad (along\ the\ C_-\ characteristic) \tag{47}$$

$$d\theta = \sqrt{M^2 - 1}\frac{dV}{V} \quad (along\ the\ C_+\ characteristic) \tag{48}$$

The Prandtl-Meyer function v(M) can be obtained by integrating the above equations[15].

$$\theta + v(M) = const = K_- \qquad (along\ the\ C_-\ characteristic) \tag{49}$$

$$\theta - v(M) = const = K_+ \qquad (along\ the\ C_+\ characteristic) \tag{50}$$

These compatibility equations provide a relation between the magnitude of velocity and direction along the characteristic lines[15].

4.1.1 *Internal Flow*

By knowing the flow field conditions at two points in the flow, the conditions at the third point can be found as shown in Fig 4.3. If the values of v_1, θ1 and v_2, θ2 are known at point 1 and point 2 respectively, the conditions at point 3 can be determined. The location of point 3 is at the intersection of C- characteristic (through point 1) and C+ characteristic (through point 2)[15].

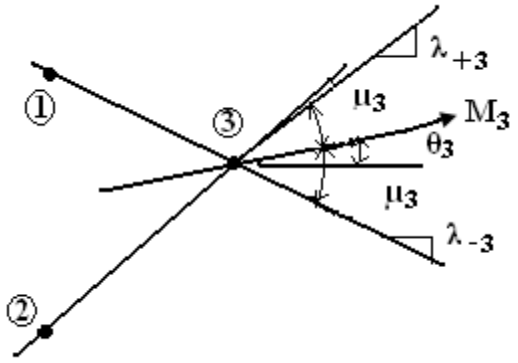

Fig 4.3 Internal points

For points 1 and 2, the K_ and K_+ are given by[15]

$$K_- = \theta_1 + v_1 \tag{51}$$

$$K_+ = \theta_2 - v_2 \tag{52}$$

Using K_ and K_+, we can calculate θ_3, v_3, μ_3, and slopes λ_{-3}, λ_{+3}

$$\theta_3 = \tfrac{1}{2}[(K_-)_1 + (K_+)_2] \tag{53}$$

$$v_3 = \tfrac{1}{2}[(K_-)_1 - (K_+)_2] \tag{54}$$

$$\mu_3 = \sin^{-1}\left(\frac{1}{M}\right) \tag{55}$$

$$\lambda_{-3} = \tan(\mu + \theta) \tag{56}$$

$$\lambda_{+3} = -\tan(\mu - \theta) \tag{57}$$

Hence, the flow conditions at point 3 are determined from the conditions at 1 and 2.

4.1.2 *Wall point*

By knowing the conditions at a point near a wall, the values of the flow variables at the wall can be determined. Consider that the flow is known at point 4 .The C- characteristic passes through point 4 where the value of K- is known. At point 5, the C- characteristics from point 4 intersect the wall. Hence the K_ value at point 5 is given by[15]

$$K_{-4} = K_{-5} = \theta_5 + \nu_5 \tag{58}$$

4.1.3 *Wave cancellation*

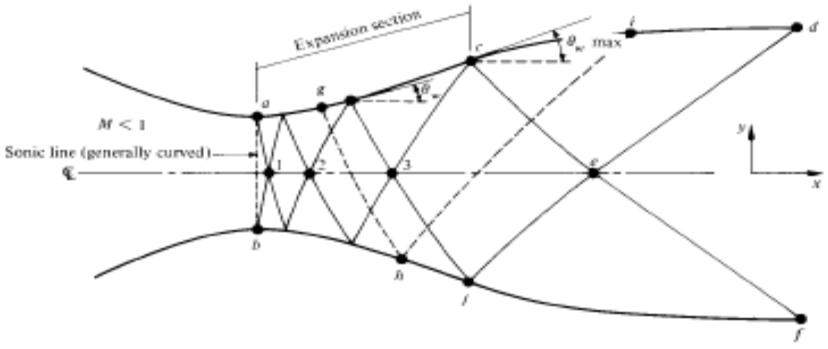

Fig 4.4 Wave cancellation[15]

The portion of the nozzle where Θ_w is increasing is known as the expansion region. The point where $\theta_w = \theta_{w_{max}}$ is called an inflection point. In the portion downstream of $\theta_{w_{max}}$ the

expansion waves generated in the expansion region will be cancelled because the θ_w decreases in this region until the contour become parallel to the x-axis. The region downstream of $\theta_{w_{max}}$ is known as a simple region because the expansion waves are cancelled at the wall[15].

4.1.4 *Position of points*

The position of points can be obtained by solving two linear algebraic equations which intersect at the point of attention[16].

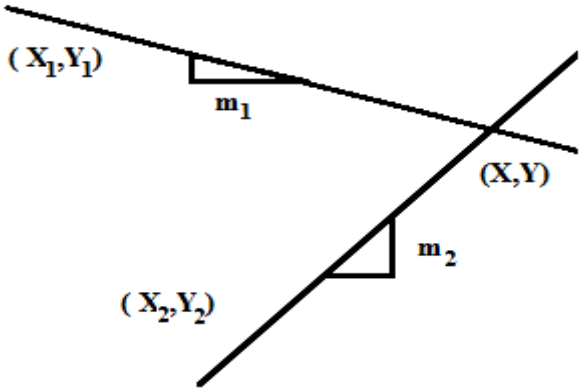

Fig 4.5 Location of points[16]

$$Y - Y_1 = m_1(X - X_1) \tag{59}$$

$$Y - Y_2 = m_2(X - X_2) \tag{60}$$

$$X = \frac{(m_2X_2 - Y_2) - (m_1X_1 - Y_1)}{m_2 - m_1} \tag{61}$$

$$Y = m_2(X - X_2) + Y_2 \tag{62}$$

As the characteristic lines are curved, the slopes m1 and m2 need to be corrected. This can be achieved by averaging the Mach slope of the previous point with the Mach slope of new point.

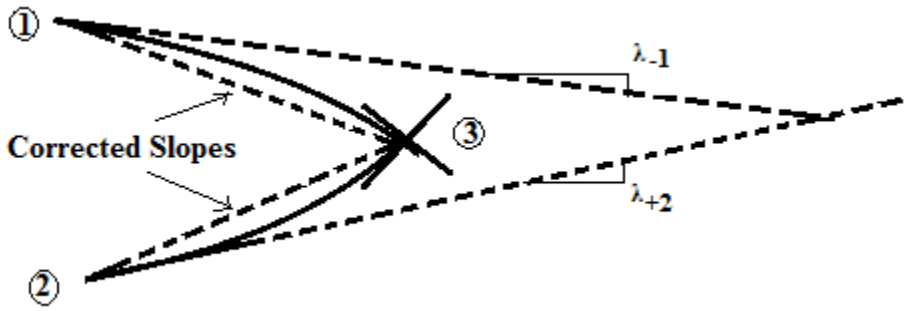

Fig 4.6 Corrected slopes for location of points[16]

$$m_1 = \tfrac{1}{2}(\lambda_{-1} + \lambda_{-3}) \tag{63}$$

$$m_2 = \tfrac{1}{2}(\lambda_{+2} + \lambda_{+3}) \tag{64}$$

For the upper surface

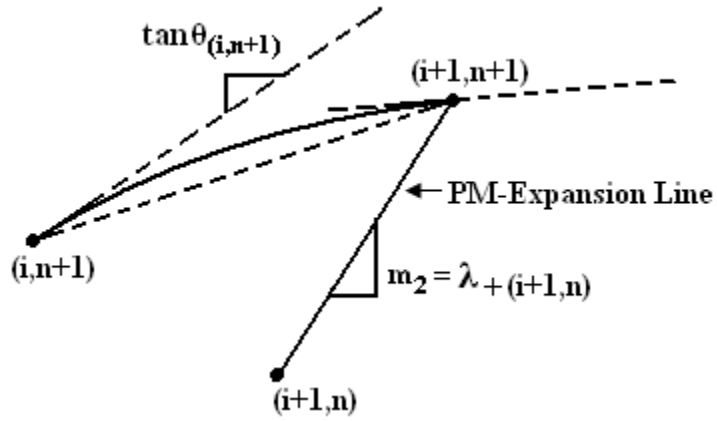

Fig 4.7 Location of upper surface points[16]

$$m_1 = \frac{1}{2}\left(\tan\theta_{(i,n+1)} + \tan\theta_{(i+1,n+1)}\right)$$

(65)

$$m_2 = \lambda_{+(i+1,n)}$$

(66)

4.1.5 *Labeling*

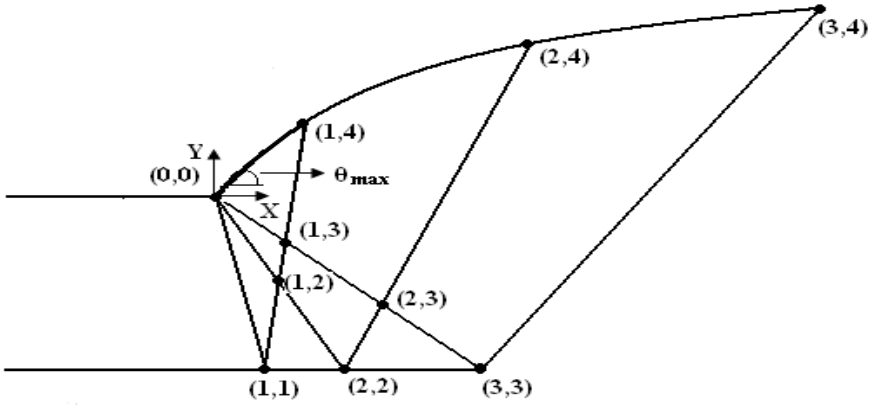

Fig 4.8 Labeling of nozzle contour[16]

The origin will be the initial turning point of the flow. Each node will have two indexes. Node (i,j) is the node where the i-th reflection C_+ characteristic intersects the j-th C_ characteristic.

4.2 Stagnation Properties of Isentropic Flow

Isentropic flow is a flow which is both adiabatic ad reversible[15]. The ratio of total to static temperature, pressure and density are given by[15]

$$\frac{T_o}{T} = 1 + \frac{\gamma - 1}{2}M^2$$

(67)

$$\frac{p_o}{p} = \left(1 + \frac{\gamma - 1}{2}M^2\right)^{\gamma/(\gamma-1)}$$

(68)

$$\frac{\rho_o}{\rho} = \left(1 + \frac{\gamma - 1}{2} M^2\right)^{1/(\gamma-1)}$$

(69)

4.3 Area –Mach number relation

The 1-D Area-Mach number relation for a nozzle is given by[15]

$$\left(\frac{A}{A^*}\right)^2 = \frac{1}{M^2}\left[\frac{2}{\gamma+1}\left(1 + \frac{\gamma-1}{2}M^2\right)^{(\gamma+1)/(\gamma-1)}\right]$$

(70)

The Mach number distribution for a desired area ratio can be obtained by using the Newton Rhapson Method[17].

$$F(M) \equiv \frac{1}{M}\left[\left(\frac{2}{\gamma+1}\right)\left(1 + \frac{(\gamma-1)}{2}M^2\right)\right]^{\frac{\gamma+1}{2(\gamma-1)}} - \frac{A}{A^*}$$

(71)

For a desired area ratio, at the correct Mach number F(M) = 0. Expanding F(M) in Taylor's series about some arbitrary Mach number $M_{(j)}$.

$$F(M) = F\left(M_{(j)}\right) + \left(\frac{\partial F}{\partial M}\right)_{(j)}\left(M - M_{(j)}\right) + \frac{\left(\frac{\partial^2 F}{\partial M^2}\right)_{(j)}\left(M - M_{(j)}\right)^2}{2} + \cdots O\left(M - M_{(j)}\right)^3$$

(72)

Then solving the above expansion for M

$$M = M_{(j)} + \frac{F(M) - F\left(M_{(j)}\right) - \left[\frac{\left(\frac{\partial^2 F}{\partial M^2}\right)_{(j)}\left(M - M_{(j)}\right)^2}{2} + \cdots O\left(M - M_{(j)}\right)^3\right]}{\left(\frac{\partial F}{\partial M}\right)_{(j)}}$$

(73)

As F(M) = 0 at correct Mach Number

$$M = M_{(j)} - \frac{F(M_{(j)}) + \left[\frac{\left(\frac{\partial^2 F}{\partial M^2}\right)_{(j)} (M - M_{(j)})^2}{2} + \cdots O(M - M_{(j)})^3\right]}{\left(\frac{\partial F}{\partial M}\right)_{(j)}} \tag{74}$$

Neglecting the higher order terms

$$\widehat{M} = M_{(j)} - \frac{F(M_{(j)})}{\left(\frac{\partial F}{\partial M}\right)_{(j)}} \tag{75}$$

4.4 Thrust

The thrust is the force produced by the propulsion system acting up on the flight vehicle. Assuming a quasi one-dimensional flow, the thrust equation for the PDE nozzle is given by

$$F_{nozzle} = I_2 - I_3 \tag{76}$$

The thrust from the PDE chamber is given by

$$F_{PDE} = I_1 - I_2 \tag{77}$$

Where,

$$I_1 = P_1 A_1 (1 + \gamma {M_1}^2) \tag{77a}$$

$$I_2 = P_2 A_2 (1 + \gamma {M_2}^2) \tag{77b}$$

$$I_3 = P_3 A_3\left(1 + \gamma {M_3}^2\right)$$

(77c)

The total thrust for the PDE is given by

$$F = F_{PDE} + F_{nozzle}$$

(78)

4.5 Mass flow rate

The mass flow rate through a nozzle is given by[18]

$$\dot{m} = \frac{AP_t}{\sqrt{T_t}}\sqrt{\frac{\gamma}{R}}M\left(1 + \frac{\gamma - 1}{2}M^2\right)^{-\frac{\gamma+1}{2(\gamma-1)}}$$

(79)

4.6 Exit velocity

The velocity at the exit of the nozzle is given by[18]

$$V_e = M_e\sqrt{\gamma R T_c\left(\frac{1}{1 + \frac{\gamma - 1}{2}{M_e}^2}\right)}$$

(80)

where

T_c = combustion chamber temperature

M_e= Mach number at the exit of the nozzle

4.7 Thrust coefficient

The thrust coefficient is a non-dimensional thrust parameter which is obtained when the thrust is divided by product of total pressure and throat area. The thrust coefficient is given by[19]

$$C_F = \gamma\sqrt{\frac{2}{\gamma-1}}\left(\frac{2}{\gamma+1}\right)^{\frac{\gamma+1}{2(\gamma-1)}}\sqrt{\left(1-\left(\frac{P_e}{P_o}\right)^{\frac{\gamma-1}{\gamma}}\right)}+\frac{A_e}{A_{th}}\left(\frac{P_e}{P_o}-\frac{P_a}{P_o}\right)$$

(81)

4.8 Overexpanded flow

The nozzle is generally designed for a particular nozzle pressure ratio. When the nozzle pressure ratio is varied below the design point nozzle pressure ratio during the off design condition the nozzle is overexpanded. In this process flow separation can occur in the nozzle because of an oblique shock wave entering in to the nozzle and causing boundary layer separation. The thrust coefficient actually increases over that predicted by inviscid theory which assumes the coalescence of oblique shock waves at the nozzle exit coalescing into a normal shock that enters the nozzle as the nozzle pressure ratio is reduced. The thrust coefficient during overexpansion of the nozzle is given by[19]

$$C_F = \gamma\sqrt{\frac{2}{\gamma-1}}\left(\frac{2}{\gamma+1}\right)^{\frac{\gamma+1}{2(\gamma-1)}}\sqrt{\left(1-\left(\frac{P_s}{P_o}\right)^{\frac{\gamma-1}{\gamma}}\right)}+\frac{A_s}{A_{th}}\left(\frac{P_e}{P_o}-\frac{P_a}{P_o}\right)$$

(82)

Where P_s= pressure at the shock-induced separation point

A_s= area at the separation point

The pressure at the separation point P_s is given by[20]

$$\frac{P_s}{P_a} = 0.583\left(\frac{P_a}{P_c}\right)^{0.195}$$

(83)

The area at the separation point A_s is given by

$$\frac{A_s}{A^*} = \frac{1}{M_s}\left[\frac{2}{\gamma+1}\left(1+\frac{\gamma-1}{2}M_s^2\right)\right]^{\frac{\gamma+1}{2(\gamma-1)}}$$

(84)

Where

$$M_s = \left[\frac{2}{\gamma - 1}\left(\left(\frac{P_c}{P_s}\right)^{\frac{\gamma-1}{\gamma}} - 1\right)\right] \tag{85}$$

CHAPTER 5

RESULTS

5.1 Design of nozzle contour for $P_e = P_a = 1$ atm

A supersonic nozzle is designed based on the method of characteristics as explained in Ref 15. The code is implemented in MATLAB and is designed for two design point conditions for $P_e = P_a = 1.0$ atm and $P_e = P_a = 0.1$ atm. The properties at the open end of the PDE as the detonation wave exits the PDE tube are taken as the initial input parameters for designing the nozzle contour.

Table 5.1 Properties at open end of the PDE for $P_e = P_a = 1.0$ atm

Combustion chamber temperature	3100 (k)
Combustion chamber pressure	2.2 (atm)
Ambient Pressure	1 (atm)
Ambient Temperature	300 (k)
Mach number	1

The nozzle contour for the selected input parameters with the number of characteristics lines n=50 for the design point $P_e = P_a = 1.0$ atm is shown in Fig 5.1. The area ratio of the nozzle contour obtained by using the method of characteristics is 1.1.

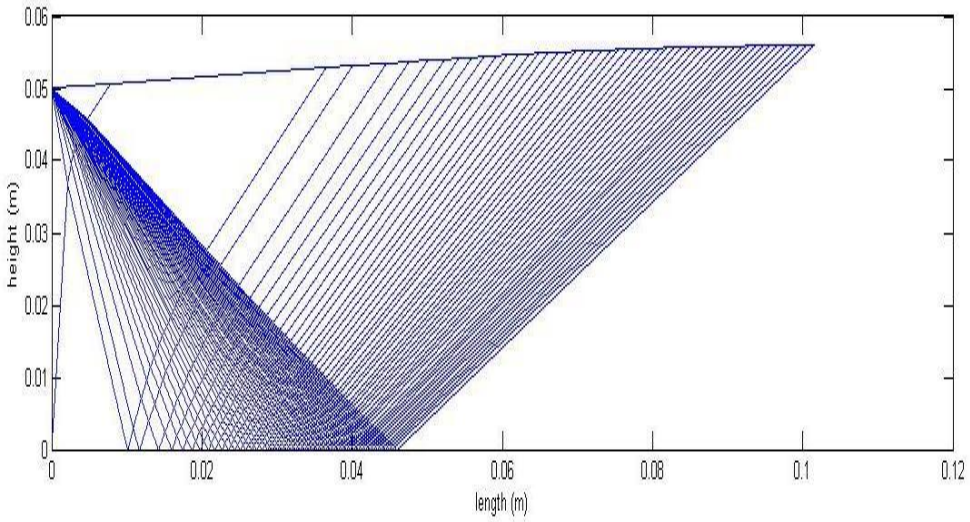

Fig 5.1 Nozzle contour for the design point $P_e = P_a = 1.0$ atm.

The variation of Mach number for the design point $P_e = P_a = 1.0$ atm is shown in Fig 5.2 below.

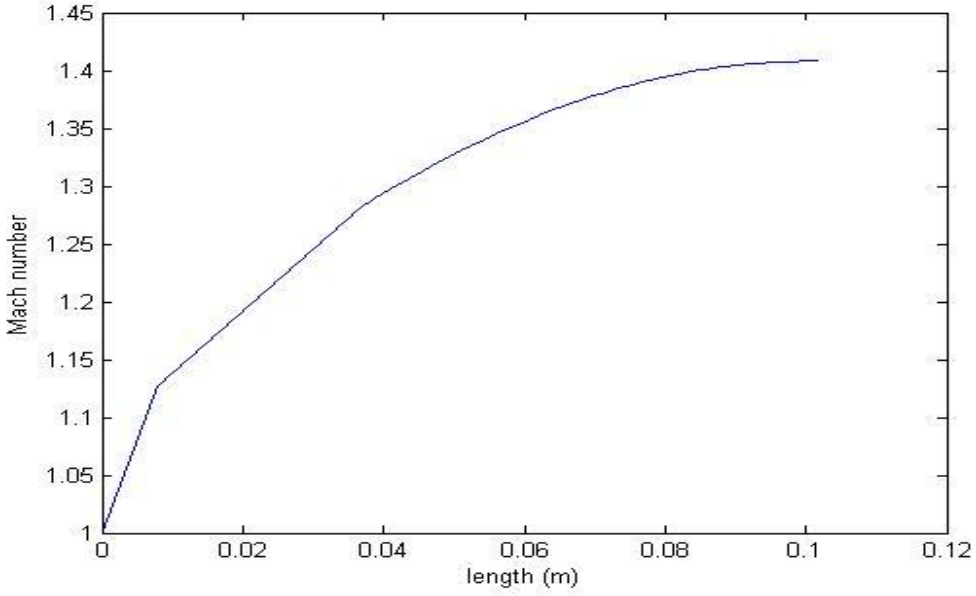

Fig 5.2 Variation of Mach number for the design point $P_e = P_a = 1.0$ atm

The nozzle thrust value obtained during the Taylor rarefaction wave process and the reflected rarefaction wave process by using the difference in impulse function $I = P\,A(1 + \gamma M^2)$ between the nozzle entrance and nozzle exit is 1503.3 N. The thrust at the end wall of PDE is calculated using the values of pressure and the area at the closed end. The pressure at the end wall P = 6.5 atm. The end wall pressure P = 6.5 atm remains constant during the Taylor rarefaction and the reflected rarefaction processes. The thrust values at the end wall of the PDE are shown in Table 5.2 below.

Table 5.2 Thrust values at the end wall of the PDE

Taylor rarefaction process (end wall)	5334.7 (N)
Reflected rarefaction process (end wall)	5334.7 (N)

The total thrust of a PDE is given by adding the thrust obtained from PDE tube and the thrust obtained from the nozzle during the Taylor rarefaction wave and reflected rarefaction wave. The total thrust values obtained during the two phases are shown in Table 5.3 below.

Table 5.3 Total thrust values during Taylor and reflected rarefaction process ($P_e = P_a$ = 1.0 atm)

Taylor rarefaction process	6838 (N)
Reflected rarefaction process	6838 (N)

The thrust during the blow down process is calculated by taking three pressure values from Table 3.8 and calculating the thrust coefficient corresponding to that pressure. The thrust coefficient values obtained during the blow down process are shown in Table 5.4 below. When the pressure P = 1.6 atm the nozzle is overexpanded and there will be a shock formation due to that as the nozzle is operating below the design point pressure ratio. The thrust coefficient value during the overexpansion is calculated by using the equation 82.

Table 5.4 Thrust coefficient values for the design point $P_e = P_a = 1$ atm

Pressure	Thrust coefficient
6.5 atm	1.166
3.7 atm	0.9980
1.6 atm	0.6402

The thrust obtained from the thrust coefficient values are shown in Table 5.5 below.

Table 5.5 Thrust values during the blow down process for $P_e = P_a = 1$ atm

Thrust coefficient	Thrust
1.166	6220.3 N
0.9980	3030.6 N
0.6402	840.7 N

The average total thrust during the blow down process of is 3363.9N. The average total thrust during the one PDE cycle (neglecting the purge and refill parts of the cycle where the thrust would be essentially zero) is found out to be 5100.9 N.

5.2 Design of nozzle contour for $P_e = P_a = 0.1$ atm

The nozzle contour for the selected input parameters with the number of characteristics lines n=50 for the design point $P_e = P_a = 0.1$ atm is shown in Fig 5.3. The area ratio of the nozzle contour obtained by using the method of characteristics is 2.99. The properties at the open end of PDE shown in Table 5.6 are taken as the initial input parameters for designing the nozzle contour.

Table 5.6 Properties at open end of the PDE for $P_e = P_a = 0.1$ atm

Combustion chamber temperature	3100 (k)
Combustion chamber pressure	2.2 (atm)
Ambient Pressure	0.1 (atm)
Ambient Temperature	300 (k)
Mach number	1

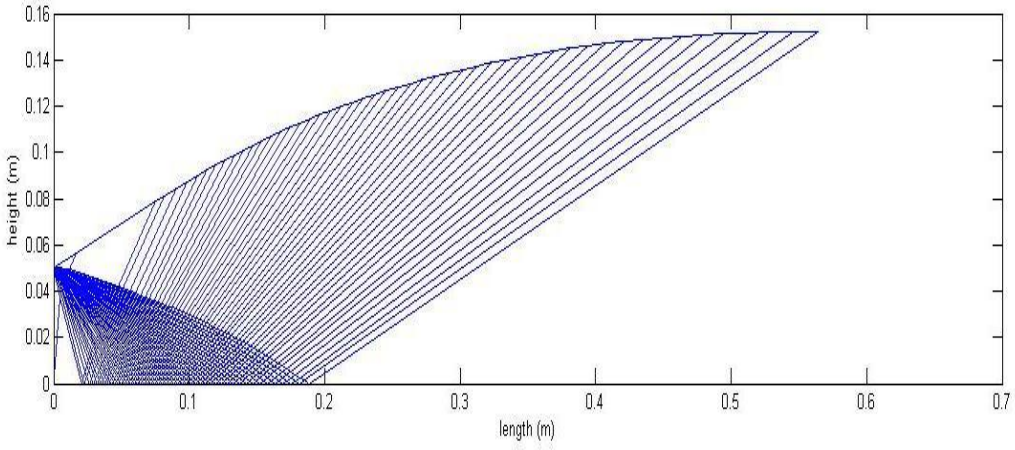

Fig 5.3 Nozzle contour for the design point $P_e = P_a = 0.1$ atm

The variation of Mach number for the design point $P_e = P_a = 0.1$ atm is show in Fig 5.4 below

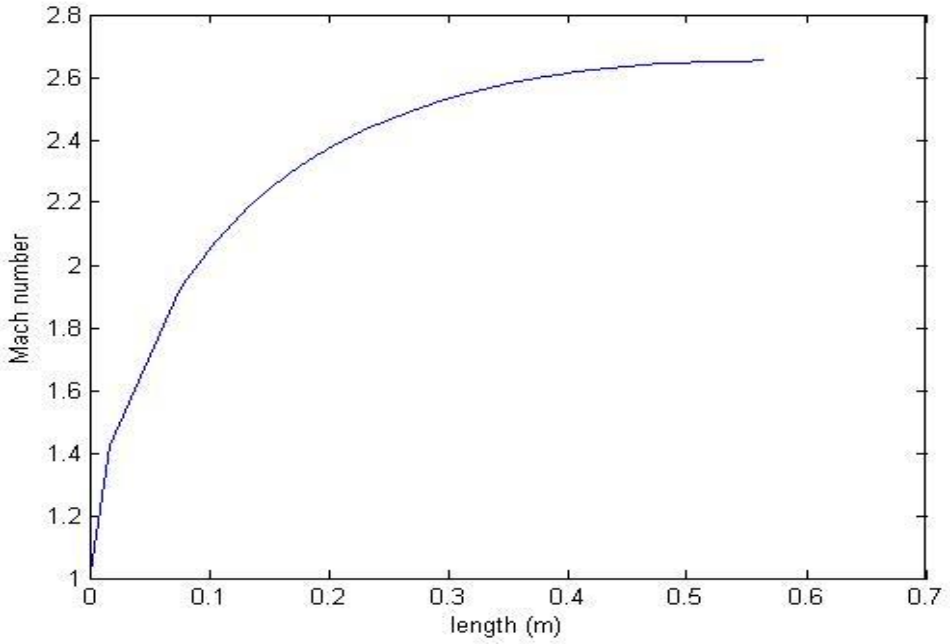

Fig 5.4 Variation of Mach number for the design point $P_e = P_a = 0.1$ atm

The nozzle thrust value obtained during the Taylor rarefaction wave process and the reflected rarefaction wave process by using the difference in impulse function $I = P\,A(1 + \gamma M^2)$ between the nozzle entrance and nozzle exit is 3921.3 N. The thrust values at the end wall of the PDE are shown in Table 5.2.

The total thrust of a PDE is given by adding the thrust obtained from PDE tube and the thrust obtained from nozzle during Taylor rarefaction wave and reflected rarefaction wave. The total thrust values obtained during the two phases are shown below in Table 5.7 below.

Table 5.7 Total thrust during Taylor and reflected rarefaction process for $P_e = P_a = 0.1$ atm

Taylor rarefaction process	9256 (N)
Reflected rarefaction process	9256 (N)

The thrust during the blow down process of one PDE cycle is calculated by taking three pressure values from Table 3.8 and calculating the thrust coefficient corresponding to that pressure. The thrust coefficient values obtained during the blow down process are shown in Table 5.8 below.

Table 5.8 Thrust coefficient values for the design point $P_e = P_a = 0.1$ atm

Pressure	**Thrust coefficient**
6.5 atm	1.33
3.7 atm	1.29
1.6 atm	1.23

The thrust values obtained from the thrust coefficient are shown in table 5.9 below.

Table 5.9 Thrust values during the blow down process for $P_e = P_a = 0.1$ atm

Thrust coefficient	**Thrust**
1.33	7095.3 N
1.29	3938.62 N
1.23	1619.2 N

The average total thrust during the blow down process of is 4217.7 N. The average total thrust during the one PDE cycle is found out to be 6736.8 N. The total thrust during the two design point considerations are shown in Table 5.10 below.

Table 5.10 Total thrust during design point pressures

Design point ($P_e = P_a = 1$ atm)	5100.9 N
Design point ($P_e = P_a = 0.1$ atm)	6736.8 N

CHAPTER 6

CONCLUSION AND FUTURE WORK

An analytical cycle analysis for the PDE was performed using a spreadsheet. The properties of the PDE cycle at different stages have been studied. The properties at different stages of the PDE cycle can be obtained by simply varying the fuel and oxidizer mixture and the initial free stream conditions. The distribution of gas properties during the Taylor rarefaction wave, reflected rarefaction wave and blow down segment of the PDE cycle are calculated. The graphs of pressure, temperature and density distributions along the length of the PDE tube are plotted to study the behavior of the Taylor rarefaction wave and reflected rarefaction wave. The average PDE pressure and temperature variations with time during the blow down phase are also calculated. The spread sheet is implemented in such a way that it can be further extended for future study.

A supersonic two-dimensional nozzle is designed by using the method of characteristics. An accurate nozzle contour can be obtained by increasing the number of characteristics lines. The average values of nozzle thrust for one PDE cycle are calculated analytically using the impulse function and thrust coefficient. The variation of PDE thrust with the change in altitude is studied by designing the nozzle for two design points.

Future work

The code can be used to optimize the design of the PDE chamber and nozzle. The PDE can be integrated with a gas turbine compressor and turbine; otherwise it can be integrated in the bypass flow of a conventional turbofan engine so that the spreadsheet can be extended and the properties of the PDE can be further investigated. A computational analysis can be done by considering different types of nozzles. The study of shock waves that may be

formed during overexpansion operation of the nozzle and interaction between the nozzle exhaust stream and the surrounding aerodynamic flow field should be investigated.

REFERENCES

1. Absolute astronomy, URL: http://www.absoluteastronomy.com/topics/Pulse_jet_engine

2. Jean-Denis G.G.Lepage “Aircraft of the Luftwaffe, 1935-1945”, McFarland & Company, Inc., 2009.

3. Nicholls, J.A., Wilkinson, H.R., Morrison, R.B., and Ong, R., “Intermittent Detonation as a Thrust-Producing Mechanism,” Progress Report No. 2, Wright Aeronautical Division, Curtiss-Wright Corporation, Jul. 1954.

4. Krzycki, L.J., “Performance Characteristics of an Intermittent Detonation Device,” NAVWEPS Report 7655, Naval Ordnance Test Station, China Lake, California, Jun. 1962.

5. Helman, D., Shreeve, R.P,, and Eidelman, S., “Detonation Pulse Engine,” Naval Post Graduate School, Monterey, California, 1986.

6. Bussing, T.R.A., Bratkovich, T.E. and Hinkey, J.B., “Practical Implementation of Pulse Detonation Engines,” AIAA-1997-2748, 33rd AIAA/ASME/SAE/ASEE Joint Propulsion Conference and Exhibit, 6-9 Jul. 1997, Seattle, WA.

7. U.S. Air Force, URL: http://www.af.mil/news/story.asp?id=123099095

8. Yunus A. Cengel and Michael Boles “Thermodynamics: An Engineering Approach”, 4th Edition, McGraw-Hill, 2001.

9. Heiser, W.H. and Pratt, D.T., “Thermodynamic Cycle Analysis of Pulse Detonation Engines,” Journal of Propulsion and Power, Vol. 18, No. 1, Jan.-Feb. 2002.

10. Maurice J.Zucrow, Joe D.Hoffman, “ Gas Dynamics” volume 1, John Wiley & Sons, Inc.,1976.

11. Kuo, K.K., “Principles of Combustion,” 2nd Ed., John Wiley and Sons, Inc., 2005.

12. Panicker, Philip K., “The Development and Testing of Pulsed Detonation Engine Ground Demonstrators,” Doctoral Dissertation, Department of Mechanical and Aerospace Engineering, The University of Texas at Arlington, Arlington, TX, 2008.

13. Takuma Endo and Toshi Fujiwara “A Simplified Analysis on a Pulse Detonation Engine Model” Tans. japan soc. Aero. Space sci Vol 44, No. 146, pp, 217-222, 2002.

14. Takuma Endo and Toshi Fujiwara “ Analytical Estimation of Performance parameters of an Ideal Pulse Detonation Engine” Tans. japan soc. Aero. Space sci Vol 45, No. 150, pp, 249-254, 2003.

15. Anderson, John D., “Modern Compressible Flow” 3rd Edition, McGraw-Hill, 2002.

16. Wilson, Dr.Donald. MAE 3303 Lecture Notes, Mechanical and Aerospace Engineering, UTA.

17. IIT Delhi, URL: http://web.iitd.ac.in/~pmvs/index.php?q=mel715.

18. NASA, URL: http://www.grc.nasa.gov/WWW/K-12/airplane/mflchk.html

19. Wilson, Dr.Donald. AE 5327 Lecture Notes, Mechanical and Aerospace Engineering, UTA.

20. RASAero, URL: http://rasaero.com/

21. Heiser, W.H. and Pratt, D.T., *Hypersonic Airbreathing Propulsion*, AIAA Education Series, Washington D.C., 1994.

BIOGRAPHICAL INFORMATION

Kishore Nekkanti was born in 1986 in India. He pursued his bachelor's degree in Aeronautical engineering from Anna University, Chennai, India in 2007. In spring 2008 he joined the University of Texas at Arlington to pursue his master's degree. He started his research work in Aerodynamics research centre (ARC) in fall 2008.